Circadian regulation of macromolecular complex turnover and proteome renewal

Authors: Estere Seinkmane[1], Anna Edmondson[1], Sew Y Peak-Chew[1], Aiwei Zeng[1], Nina M Rzechorzek[1], Nathan R James [1], James West[2], Jack Munns [1], David CS Wong[1], Andrew D Beale*[1], John S O'Neill*[1]

[1]MRC Laboratory of Molecular Biology, Francis Crick Avenue, Cambridge, CB2 0QH

[2]Department of Medicine, University of Cambridge, UK

*correspondence to: oneillj@mrc-lmb.cam.ac.uk, abeale@mrc-lmb.cam.ac.uk

ABSTRACT

Although costly to maintain, protein homeostasis is indispensable for normal cellular function and long-term health. In mammalian cells and tissues, daily variation in global protein synthesis has been observed, but its utility and consequences for proteome integrity are not fully understood. Using several different pulse-labelling strategies, here we gain direct insight into the relationship between protein synthesis and abundance proteome-wide. We show that protein degradation varies in-phase with protein synthesis, facilitating rhythms in turnover rather than abundance. This results in daily consolidation of proteome renewal whilst minimising changes in composition. Coupled rhythms in synthesis and turnover are especially salient to the assembly of macromolecular protein complexes, particularly the ribosome, the most abundant species of complex in the cell. Daily turnover and proteasomal degradation rhythms render cells and mice more sensitive to proteotoxic stress at specific times of day, potentially contributing to daily rhythms in the efficacy of proteasomal inhibitors against cancer. Our findings suggest that circadian rhythms function to minimise the bioenergetic cost of protein homeostasis through temporal consolidation of protein turnover.

Introduction

Protein homeostasis, or proteostasis, refers to the dynamic process of maintaining protein abundance and functionality. It involves regulation of synthesis, folding, localisation and degradation of proteins, such that the appropriate proteins are present within the appropriate concentration range, in the correct compartment, at the right time. Multiple quality control and stress response mechanisms function to preserve proteome integrity over multiple timescales (Wolff *et al*, 2014; Harper & Bennett, 2016) whereas failure of proteostasis networks is strongly associated with impairment of cell function as well as ageing-related pathological states such as neurodegeneration (Labbadia & Morimoto, 2015; Hipp *et al*, 2019). By contrast, priming of proteostatic pathways enhances cellular resistance to proteotoxic stress (Rzechorzek *et al*, 2015).

Most aspects of mammalian cellular and organismal physiology are regulated over a circadian (about daily) timescale to anticipate the differing demands of day and night (Dibner *et al*, 2010; Atger *et al*, 2017). Whilst circadian rhythms are generated cell autonomously (Welsh *et al*, 2004; Yoo *et al*, 2004), *in vivo,* myriad cellular clocks throughout the body are synchronised with daily environmental cycles by systemic timing cues. For example, daily rhythms of feeding entrain cellular clocks through the insulin signalling pathway to stimulate PERIOD "clock protein" production *via* activation of mammalian target of rapamycin complexes (mTORCs) (Crosby *et al*, 2019). Daily rhythms of PERIOD and mTORC activity facilitate daily rhythms of gene expression and protein synthesis. In particular, mTORC1 is a master regulator of bulk 5'-cap-dependent protein synthesis, degradation and ribosome biogenesis (Valvezan & Manning, 2019) whose activity is circadian-regulated in tissues and in cultured cells (Ramanathan *et al*, 2018; Feeney *et al*, 2016a; Stangherlin *et al*, 2021b; Mauvoisin *et al*, 2014; Jouffe *et al*, 2013; Sinturel *et al*, 2017; Cao, 2018). It is plausible that daily rhythms of mTORC activity underlie many aspects of daily physiology (Crosby *et al*, 2019; Stangherlin *et al*, 2021a; Beale *et al*, 2023b).

Most models for circadian regulation of mammalian cell function have suggested that daily rhythms in the transcription of 'clock-controlled genes' leads to daily rhythms in the abundance, and thus activity, of the encoded protein (Cox & Takahashi, 2019; Zhang *et al*,

2014; Andreani *et al*, 2015). However, recent -omics approaches, which measure many thousands of individual transcripts and proteins, have revealed multiple discrepancies with this abundance-based hypothesis, such as poor correlations between mRNA and encoded protein abundance (Stangherlin *et al*, 2021a). Moreover, the rather modest extent of daily changes in protein abundance (typically < 20%), and poor reproducibility between independent studies (Janich *et al*, 2015; Mauvoisin *et al*, 2014; Reddy *et al*, 2006; Robles *et al*, 2014; Mauvoisin & Gachon, 2020; Brooks *et al*, 2023), suggests that physiological variation in protein abundance is unlikely to account for large daily variations in multiple biological functions observed in tissues and cultured cells. Indeed, daily cycles of protein abundance would appear contrary to the essential requirement for maintaining proteostasis, which the major fraction of cellular energy budgets are spent to sustain (Buttgereit & Brand, 1995; Lane & Martin, 2010).

Compelling evidence for physiological daily variation in global rates of protein synthesis cannot be ignored, however (Lipton *et al*, 2015; Feeney *et al*, 2016a; Stangherlin *et al*, 2021b). Such observations are difficult to reconcile with linked observations that, excepting feeding-driven changes in mouse liver, total cellular volume and protein levels show little daily variation (Stangherlin *et al*, 2021b; Hoyle *et al*, 2017; Sinturel *et al*, 2017). To resolve these apparent discrepancies we have proposed that, in non-proliferating cells, daily changes in protein synthesis are accompanied by changes in protein degradation (Stangherlin *et al*, 2021a), resulting in daily cycles of protein turnover. This further predicts that daily rhythms in protein turnover prevail over rhythms in protein abundance to favour rhythmic proteome renewal over compositional variation. Daily turnover rhythms would be particularly beneficial for coordinated biogenesis of multiprotein complexes, since complex assembly requires individual subunits to be present stoichiometrically at the same time, in the same cellular compartment, or else be wastefully degraded (Juszkiewicz & Hegde, 2018; Taggart *et al*, 2020).

Here, we aimed to test these predictions by investigating circadian regulation of global protein synthesis and degradation, as well as macromolecular complex turnover, specifically. In so doing, we utilised bulk pulse-chase labelling to establish proof-of-principle, before developing a novel time- and cellular fraction- resolved dynamic mass spectrometry

91 approach that provides the first direct and simultaneous measurements of protein synthesis
92 and abundance proteome-wide. To validate our findings, we then tested for rhythmic
93 macromolecular complex turnover directly, by quantification of nascent ribosome complex
94 assembly through the combination of heavy uridine pulse-labelling of nascent RNA with
95 ribosome purification. Given its importance in health and disease, we also aimed to
96 investigate the functional consequences of rhythmic proteostasis regulation, revealing time-
97 of-day-dependent differential sensitivity to proteotoxic stress in both cells and mice.
98

Results

Phase-coherent global rhythms in protein synthesis and degradation

We first asked whether there was any indication of cell-autonomous daily variation in protein turnover in confluent cultures of non-transformed quiescent lung fibroblasts derived from mice expressing the rhythmic luciferase reporter PER2::LUC. Using this cellular model under constant conditions, longitudinal bioluminescence recordings from parallel replicate cultures can be used to provide a robust report of cell-autonomous circadian timekeeping and establish circadian phase (Yoo *et al*, 2004; Feeney *et al*, 2016b). To measure protein degradation in parallel with synthesis, and thus assess the level of protein turnover, we first employed a traditional ^{35}S-methionine/cysteine pulse-chase labelling strategy (15 min pulse, 60 min chase).

The experiment was performed over a 24h time series followed by soluble protein extraction using digitonin, which preferentially permeabilises the plasma membrane over organelle membranes. For pulse alone, ^{35}S incorporation varied significantly over this period (Fig 1A, B, S1A), consistent with previous reports of rhythmic protein synthesis (Stangherlin *et al*, 2021b; Lipton *et al*, 2015; Zhuang *et al*, 2023). As expected, ~20% of nascently synthesised proteins had been degraded after 1 hour of chase, representing rapid quality control-associated proteasomal degradation of orphan subunits as well as aberrant translation products due to premature termination and/or protein misfolding (Schubert *et al*, 2000; Wheatley *et al*, 1980; Harper & Bennett, 2016). Importantly, the proportion of degraded protein varied over time, being highest at around the same time as increased protein synthesis (Fig 1B), indicating time-of-day variation in digitonin-soluble protein turnover which cannot be solely attributed to previously reported circadian regulation of protein solubility (Stangherlin *et al*, 2021b). Rather, it suggests that global rates of protein degradation may be co-ordinated with protein synthesis rates, and may vary over the circadian cycle.

Quality control-associated degradation predominantly occurs via the ubiquitin-proteasome system (UPS) (Schubert *et al*, 2000; Wang *et al*, 2013). To directly test whether the global

rate of proteasomal protein degradation is under circadian control, as suggested previously (Desvergne *et al*, 2016; Ryzhikov *et al*, 2019; Hansen *et al*, 2021), we employed biochemical in-cell assays for proteasomal activity at discrete biological times over the circadian cycle. Over two days under constant conditions we observed a significant ~24h oscillation in proteasomal trypsin-like and chymotrypsin-like activities of the proteasome, but not caspase-like activity (Fig 1C). Moreover, we detected a significant interaction between genotype and biological time when comparing trypsin-like proteasome activity between wild type and Cryptochrome1/2-deficient cells, that lack canonical circadian transcriptional feedback repression (Fig S1B, (Wong *et al*, 2022)). Previous proteomics studies under similar conditions have revealed minimal circadian variation in proteasome subunit abundance (Wong *et al*, 2022), suggesting that proteasome activity rhythmicity, and therefore rhythms in UPS-mediated protein degradation, are regulated post-translationally (Marshall & Vierstra, 2019; Hansen *et al*, 2021).

If global rates of proteasome-mediated protein degradation vary in phase with protein synthesis over the circadian cycle, this would result in circadian organisation of nascent protein turnover. To validate this, we employed puromycin, an antibiotic which is incorporated into nascent polypeptides by both elongating and stalled ribosomes (Nathans, 1964; Semenkov *et al*, 1992) thus making these peptides amenable to immunodetection (Aviner, 2020; Goodman & Hornberger, 2013; Schmidt *et al*, 2009). Unlike ^{35}S-labelled and other amino acid analogues, puromycin can be added to cell media directly, without the need to remove endogenous amino acids, thereby minimising acute perturbations. Whilst most studies have used puromycin incorporation as a proxy for translation rate, we reasoned that protein degradation should also affect the observed levels of puromycylated peptides, as these peptides are prematurely terminated and are thus identified and degraded rapidly by the ubiquitin-proteasome system (Lacsina *et al*, 2012; Szeto *et al*, 2006). Acute (30 min) puromycin treatment of cells in culture, with or without proteasomal inhibition (by bortezomib, BTZ), allowed us to measure both total nascent polypeptide production (+BTZ) and the amount of nascent polypeptides remaining when the UPS remained active (-BTZ). This allowed inference of the level of UPS-mediated degradation of puromycylated peptides within each time window, as a proxy for nascent protein turnover (Fig 1D).

As determined by anti-puromycin western blots, over two days under constant conditions, puromycin incorporation in the presence of BTZ showed significant circadian variation. In contrast, cells that were treated with puromycin alone showed no such variation, and nor did total cellular protein levels (Fig 1E, Fig S2A). These observations support the possibility that phase-coherent daily rhythms in protein degradation might act in parallel with rhythms in translation rate, such that the proportion of degraded peptides vary in synchrony with those that were translated (Fig 1E).

Protein synthesis is the most energetically expensive process that most cells undertake (Buttgereit & Brand, 1995; Lane & Martin, 2010). *In vivo*, the temporal consolidation of global translation might be expected to confer a fitness advantage by organising this energetically expensive process to coincide with the biological time of greatest (anticipated) nutrient availability. In nocturnal mice, for example, hepatic ribosome biogenesis preferentially occurs at night, during the active/feeding phase (Jouffe *et al*, 2013; Jang *et al*, 2015; Sinturel *et al*, 2017). To explore the physiological relevance of our cellular observations, we adapted the puromycin ± BTZ labelling strategy *in vivo*, to test the specific prediction that nascent protein turnover is increased during the active phase compared with the rest phase. In livers isolated from mice at opposite times of day, we observed significantly higher turnover during the night (active/feeding phase, ZT13), compared with the daytime (rest/fasting phase, ZT1) (Fig 1F, Fig S2B). We suggest that both in cells and in mouse liver *in vivo*, the daily variation in nascent protein turnover could be an expected consequence of imperfect translation, which requires ubiquitous protein quality control mechanisms to shield the proteome from defective, misfolded, or orphaned (excess subunit) proteins.

Proteome-wide investigation of circadian protein synthesis, abundance, and turnover

Beyond protein quality control, Figure 1 invited us to consider how circadian regulation of global protein degradation might interact with rhythmic synthesis to impact proteome composition more broadly, at the level of individual proteins. In the simplest scenario, protein abundance would correlate with synthesis rate; however, rhythmic degradation

might attenuate variation in the abundance of rhythmically synthesised protein, or alternatively it may generate variation in the abundance of constitutively synthesised proteins. We devised a novel proteome-wide approach to test each of these scenarios.

To measure protein production and abundance simultaneously and directly over the circadian cycle, we utilised pulsed stable isotopic labelling with amino acids in culture (pSILAC), in combination with TMT-based mass spectrometry quantification to allow multiplexed measurements. Although pSILAC is normally applied continuously and protein harvested at multiple points to measure half-life (Doherty *et al*, 2009; Schwanhäusser *et al*, 2011; Ross *et al*, 2021), here we used a repeated fixed time window for SILAC labelling to measure newly-synthesised proteins (Fig 2A, B). To enable sufficient heavy labelling for detection, a 6h time window was employed, thus measuring synthesis and abundance within each quarter of the circadian cycle.

Over our 48h time series, we reliably detected heavy peptides for 2528 unique proteins from whole cell lysates, representing estimates of their synthesis at each time window, and compared this with their total abundance calculated from the sum of heavy and light peptides (Supplementary Table 1; examples in Fig 2C). The specific number or proportion of rhythmically synthesised and/or abundant proteins is expected to vary with detection method (Hughes *et al*, 2017; Mei *et al*, 2021) and may be susceptible to overestimation of rhythmicity. We therefore employed several methods, including less stringent RAIN and more stringent ANOVA, to compare the extent of temporal variation in protein synthesis and total abundance (Fig 2D, E).

Consistent with similar previous studies, <10% of detected proteins showed any significant variation over the circadian cycle (Fig 2E). This is also expected considering the long average half-life (~days) of mammalian proteins (Mathieson *et al*, 2018; Schwanhäusser *et al*, 2011; Wong *et al*, 2022). Amongst those with significant temporal variation, we found that similar proportions of the proteome showed rhythms in synthesis as rhythms in abundance (Fig 2E). Of the rhythmically abundant proteins, a minority showed accompanying rhythms in synthesis, with no difference in phase (Fig 2E, F). The proportion of such proteins was more than expected by chance ($p<0.0001$, Fisher's Exact Test), and their behaviour aligns with the

canonical "clock-controlled gene" paradigm, in which physiological rhythms are proposed to arise through circadian variation in protein abundance, generated *via* transcriptional and translational oscillations. Strikingly however, the majority of rhythmically synthesised proteins showed no accompanying rhythm in abundance and *vice versa* (Fig 2E). Moreover, the extent of daily synthesis variation (fold change) was significantly greater than abundance (Fig 2D). These observations are consistent with our model of widespread temporal organisation of protein degradation within the circadian-regulated proteome.

Considering all detected proteins that were either rhythmically synthesised or rhythmically abundant, peaks occurred in all four quarters of the cycle (Fig 2G), but clustered in the quarter of the cycle immediately after the peak of PER2::LUC, in accordance with proteome-wide rhythms (Fig 1A, B). Gene ontology analysis did not reveal functional enrichment for any particular biological process or compartment in either group compared with background.

Targeted investigation of circadian protein synthesis, abundance, and turnover

The experiment above was designed to combine and compare two time-resolved processes — that of circadian variation and that of protein production — and so only considered proteins with reliably detectable heavy label incorporation within a given labelling window (6h) across all timepoints. This inevitably limited and biased the proteome coverage towards abundant proteins with higher synthesis rates, irrespective of cellular compartment or function. This probably explains the absence of functional enrichment among rhythmic proteins that have been observed in other studies, as well as the lower level of overall variation in synthesis than would be expected from the bulk labelling investigations.

To gain more insight into the dynamics of circadian proteomic flux, we refined our pSILAC approach, this time focusing on proteins in complexes. Specifically, we aimed to test the hypothesis that circadian control of translation and turnover facilitates the coordinated assembly of multiprotein complexes (Taggart *et al*, 2020; O'Neill *et al*, 2020; Stangherlin *et al*, 2021a). To achieve this, we utilised and adjusted LOPIT-DC protocol (Geladaki *et al*, 2019) which was developed to separate different cellular compartments and fractions, to isolate

the macromolecular complex (MMC) fraction *via* gentle cell lysis followed by sequential ultracentrifugation.

To further improve the sensitivity of our pSILAC method to circadian differences, especially those occurring among most recently synthesised proteins, we also employed a shorter pulse (1.5h). To compensate for the shorter pulse and the fractionation, which otherwise would have resulted in decreased coverage, especially of the heavy peptides, we employed further technical improvements. Namely, we added a so-called booster channel: an additional fully heavy-labelled cell sample within a TMT mixture (Klann *et al*, 2020). When the mixture is analysed by MS, heavy peptides from the booster channel increase the overall signal of all identical heavy peptides at MS1 level; at MS2 and MS3 this results in improved detection of heavy proteins in the other TMT channels of interest, and is particularly advantageous for the proteins with lower turnover that would fall below the MS1 detection limit without the booster.

With this new design, heavy peptides within the enriched MMC fraction were quantified across two days (as for the first pSILAC experiment), representing proteins synthesised within 1.5h at each timepoint (Fig 3A, B, Supplementary Table 2). Despite enriching for only one cellular compartment, the overall coverage in this experiment was similar to the previous one (6577 and 6264 proteins, respectively), due to the altered and more targeted approach; with heavy peptides detected for 2302 proteins. There was a significant circadian variation among the overall amount of heavy labelled peptides that was consistent with rhythmic production of nascent proteins, whereas the total protein level in this fraction showed no change over time (Fig S3A, B).

Using boosted fractionated pSILAC, we immediately noticed a 3-fold increase in the proportion of proteins that varied significantly over time in their synthesis as compared to the whole-cell level, regardless of algorithm used (Fig 3C). The production of rhythmically synthesised proteins in this fraction also varied over time to a far greater extent than did their abundance (~2-fold greater variation, Fig 3D). Moreover, we found that a much higher proportion of detected proteins exhibited rhythms in both synthesis and total abundance than was observed at the whole-cell level (Fig 3E). As in whole-cell, the proportion of

proteins showing rhythmic synthesis but not abundance and *vice versa*, was much greater than expected by chance ($p<0.0001$, Fisher's Exact Test). By inference therefore, the proportion of proteins that are rhythmically degraded in this fraction must equal or exceed the proportion that are rhythmically synthesised. It is also noteworthy that although there were small sets of proteins that were rhythmic in both whole-cell (Figure 2) and MMC fractions (Figure 3), in both synthesis and total abundance, none of these four overlaps were higher than would have been expected by chance.

Analysis of the proteins in the MMC fraction revealed 243 annotated multiprotein complexes (from CORUM, COMPLEAT and manual annotation (Ori *et al*, 2016; Giurgiu *et al*, 2019)) to be present, including 82 complexes for which half or more annotated subunits were detected (Supplementary Table 3). It has previously been shown that protein subunits within the same complex tend to share similar turnover rates, which is thought to facilitate their co-ordinated assembly and removal (Price *et al*, 2010; Mathieson *et al*, 2018). We observed this in our data (Fig S3C) but can also add a temporal dimension: for complexes such as ribosomes, RNA polymerase, chaperonin (CCT) complex and others, the majority of component subunits not only showed similar average heavy to total protein ratios but also a similar change in synthesis over the daily cycle (Fig 3F, S3D and E). This supports the hypothesis that the assembly and turnover of macromolecular protein complexes is under circadian control.

Using an alternative approach to estimate the importance of rhythmicity for interactions of proteins within complexes, we took advantage of the STRING protein-protein interaction database (Szklarczyk *et al*, 2021). Unlike proteins with rhythmic synthesis at the whole-cell level, rhythmic proteins in this complex fraction had significantly more annotated physical interactions than would have been expected by chance given all proteins detected (Fig 3G, Fig S4). Importantly, these rhythmically synthesised protein subunits were almost all clustered within the same circadian phase (see Figure 4, discussed below).

To validate these observations by an orthogonal method, we pulse-labelled cells with methionine analogue L-azidohomoalanine (Dieterich *et al*, 2006). AHA is an exogenous substrate, with a lower affinity for methionyl-tRNA synthetase than methionine, whose

incorporation into polypeptide chains could potentially impact the stability of labelled proteins (Ma & Yates, 2018). We therefore only used AHA to assess nascent complex synthesis, rather than turnover. We analysed the incorporation of the newly synthesised, AHA labelled proteins into highest molecular weight protein species detected under native-PAGE conditions (Fig 3H, S3F). We observed a high amplitude daily rhythm of AHA labelling, indicating the rhythmic translation and assembly of nascent protein complexes. Taken together, these results show that daily rhythms in synthesis and degradation may be particularly pertinent for subunits of macromolecular protein complexes.

Temporal consolidation of biological functions

Within the MMC fraction, we found that the vast majority of rhythmically synthesised proteins showed highest synthesis at the same biological time, shortly after the peak of the PER2::LUC circadian bioluminescence reporter. Gene ontology analysis of these proteins (compared with a background list of all proteins detected in this fraction) revealed a clear enrichment for RNA binding proteins and terms associated with ribosome assembly (Fig 4A). At the same circadian phase, rhythmically abundant proteins were similarly enriched for terms relating to RNA binding and ribonucleoprotein biogenesis, as well as many proteins associated with stress granule assembly, such as ataxin-2 and many DDX family members (Fig 4A,B). Ribosomes and stress granules themselves control protein synthesis and regulate each other, so it is challenging to ascribe causal relationships between the two (Buchan & Parker, 2009; Riggs *et al,* 2020; Delarue *et al,* 2018) but our analysis clearly suggests a cell-autonomous surge of ribosome biogenesis.

Rhythmically synthesised/abundant proteins belonging to classes associated with ribonucleoproteins did not exhibit commensurate total abundance oscillations at the whole-cell level (Fig 2, Fig 4B, Supplementary Table 1; (Wong *et al,* 2022; Hoyle *et al,* 2017)), and this might indicate that some abundance variation in the MMC fraction arises from redistribution between lighter and denser fractions over the circadian cycle, consistent with circadian regulation of protein solubility and compartmentalisation described previously (Wang *et al,* 2019; Stangherlin *et al,* 2021b; Jang *et al,* 2015; Malcolm *et al,* 2019; Zhuang *et al,* 2023). Supporting this possibility, we noted a smaller group of rhythmically abundant

355 proteins in the phase preceding ribosome biogenesis, without any accompanying change in
356 synthesis. These proteins were enriched by 9-fold for actin and associated regulators of the
357 actin cytoskeleton (q<0.05, Fig 4A, C). This is consistent with circadian regulation of
358 cytoskeletal dynamics and actin polymerisation that we and others have described
359 previously (Hoyle *et al*, 2017; Gerber *et al*, 2013). Indeed, as one of the most abundant
360 cellular proteins, by mass alone, beta-actin accounted for 67% of the temporal
361 compositional variation in the phase preceding ribosome biogenesis (Supplementary Table
362 2).
363
364 **Circadian regulation of ribosome turnover not abundance**
365
366 The ribosome is by far the most abundant macromolecular complex in the cell (An & Harper,
367 2020) and showed clear evidence of circadian regulation of turnover but not abundance at
368 the whole-cell level in our pSILAC proteomics. To validate this result, we took advantage of
369 two important observations: (1) all fully assembled ribosomes incorporate ribosomal RNA
370 (rRNA) which can be readily separated from most other cellular RNA by density gradient
371 centrifugation; (2) pulse-labelling with heavy uridine-$^{15}N_2$ allows nascent RNA to be
372 distinguished from pre-existing RNA. RNA could then be nuclease-digested, and the ratio of
373 light to heavy uridine 5′-monophosphate (UMP) quantified by mass spectrometry. By
374 combining this stable isotope labelling with ribosome purification, we developed a novel
375 cellular assay which we could use to identify nascently assembled ribosomes (Fig 5A).
376 Circadian variation in the proportion of heavy UMP-containing assembled ribosomes,
377 without an accompanying variation in total UMP abundance would directly demonstrate
378 rhythmicity in ribosomal turnover.
379
380 In line with this prediction, over a circadian time series under constant conditions, we
381 observed an approximately 24 h oscillation in the percentage of heavy UMP detected within
382 assembled ribosomes (Fig 5B). We found the highest rates of assembly occurred after the
383 peak of PER2::LUC bioluminescence (Fig 5B), in line with pSILAC (Fig 3F). In addition, we
384 observed an oscillation of heavy UMP in total RNA, likely due to rRNA which comprises
385 >80% of total cellular RNA (Blobel & Potter, 1967; Palazzo & Lee, 2015). Importantly, total
386 UMP within assembled ribosomes did not change significantly over time and nor did total

cellular RNA (Fig 5B), providing further evidence for circadian regulation of macromolecular complex turnover rather than abundance, in line with our MMC fraction pSILAC results.

Rhythmic response to proteotoxic stress in cells and in mice

Disruption of proteostasis and sensitivity to proteotoxic stress are strongly linked with a wide range of diseases (Wolff *et al*, 2014; Harper & Bennett, 2016; Labbadia & Morimoto, 2015; Hipp *et al*, 2019). Evidently, global protein translation, degradation and complex assembly are crucial processes for cellular proteostasis in general, so cyclic variation in these processes would be expected to have (patho)physiological consequences. Elevated levels of misfolded, unfolded, or aggregation-prone proteins perturb proteostasis and provoke proteotoxic stress responses that disrupt cellular function, leading to cell death unless resolved (Santiago *et al*, 2020; Deshaies, 2014). Informed by our observations, we predicted that circadian rhythms of global protein turnover would have functional consequences for maintenance of proteostasis. Specifically, we expected that cells would be differentially sensitive to perturbation of proteostasis induced by proteasomal inhibition using small molecules such as MG132 and BTZ, depending on time-of-day.

We first assessed the phosphorylation status of eIF2α, the primary mediator of the integrated stress response (ISR) pathway, throughout a full circadian timecourse in fibroblasts under unperturbed versus stress-induced conditions. As expected, acute proteasomal inhibition by 4h treatment with MG132 induced eIF2α phosphorylation (Jiang & Wek, 2005), but importantly this induction varied depending on time of drug treatment (Fig 6A, S5A), with highest fold-change increase observed around the predicted peak of protein turnover (shortly after the PER2::LUC peak). Phosphorylation of eIF2α leads to inhibition of canonical translation and is suggested to drive a daily decrease in bulk protein synthesis *in vivo* (Karki *et al*, 2020; Wang *et al*, 2019; Pathak *et al*, 2019). We did not observe any cell-autonomous rhythm in eIF2α phosphorylation under basal conditions (Fig S5A), and so suggest that daily p-eIF2α rhythms observed *in vivo* likely arise through the interaction between cell-autonomous mechanisms and daily cycles of systemic cues, e.g. insulin/IGF-1 signalling and body temperature rhythms driven by daily feed/fast and rest/activity cycles respectively (Crosby *et al*, 2019; Beale *et al*, 2023a).

A major detrimental consequence of proteotoxic stress is formation of insoluble intracellular protein aggregates (Albornoz *et al*, 2019; Dantuma & Lindsten, 2010). To test whether this was also time-of-day dependent, we used a molecular rotor dye that becomes fluorescent upon intercalation into quaternary structures associated with protein aggregates (Shen *et al*, 2011) (Fig S5B). As predicted, over two days, challenging cells with MG132 around the peak of protein turnover resulted in significantly more protein aggregation compared to controls than the same challenge delivered 12 h later (Fig 6B, S5C).

Sustained proteotoxic stress results in cell death (Santiago *et al*, 2020; Deshaies, 2014), and cell death induced by 6h treatment with BTZ showed a clear circadian rhythm (Fig 6C). Strikingly, we found roughly twice as much cell death occurred for proteasomal inhibition at the peak of protein turnover compared with its nadir (Fig 6C, S5D). In contrast, translational inhibition with cycloheximide revealed no such temporal variation. Together, these data support our predictions, wherein proteasomal inhibition at peak times of translation and protein turnover exacerbates proteotoxic stress, protein aggregation, and cell death because the burden on protein quality control systems at these circadian phases is already high.

BTZ and its derivatives are used clinically to treat several types of blood cancers, associated with a multitude of side effects due to the proteasome's essential function in all cells (Deshaies, 2014; Manasanch & Orlowski, 2017; Zhang *et al*, 2020). In light of the daily variation in protein turnover we observed in mouse liver (Fig 1F), we hypothesised that time-of-day sensitivity to BTZ would also be observed *in vivo*. Accordingly, we observed a stark day vs night difference in the response to BTZ treatment in mouse liver, assessed by eIF2α phosphorylation (Fig 6D-F, Fig S5E). Consistent with this, time-of-day variation in BTZ-mediated inhibition of tumour growth was recently demonstrated in a mouse tumour model study (Wagner *et al*, 2021).

Discussion

In this work, we provide evidence for coordinated circadian regulation of protein synthesis and degradation, resulting in rhythmic protein turnover, which is particularly significant for macromolecular complexes such as the ribosome. Across all experiments in this study, we find that protein synthesis, degradation and turnover is highest during the 6-8h that follow maximal production of the clock protein PER2. This is coincident with increased glycolytic flux and respiration (Putker *et al*, 2018), increased macromolecular crowding in the cytoplasm, decreased intracellular K^+ concentration and increased mTORC activity (Feeney *et al*, 2016a; Stangherlin *et al*, 2021b; Wong *et al*, 2022). Just as temporal consolidation of protein synthesis is thought to increase its metabolic efficiency (O'Neill *et al*, 2020), we suggest that rhythmic turnover may serve to increase the efficiency of proteostasis by minimising deleterious changes in total cellular protein content and proteome composition.

The mechanistic underpinnings for cell-autonomous circadian regulation of the translation and degradation machineries remain to be fully explored, but are likely to be driven by daily rhythms in the activity of mTORC: a key regulator of protein synthesis and degradation as well as macromolecular crowding and sequestration (Stangherlin *et al*, 2021b, 2021a; Cao, 2018; Adegoke *et al*, 2019; Ben-Sahra & Manning, 2017; Delarue *et al*, 2018). In particular, global protein synthesis rates are greatest when mTORC1 activity is highest, in tissues and cultured cells, whereas pharmacological treatments that inhibit mTORC1 activity reduce daily variation in crowding and protein synthesis rates (Feeney *et al*, 2016a; Lipton *et al*, 2015; Stangherlin *et al*, 2021b). Given our focus on proteomic flux and translation-associated protein quality control, autophagy was not directly within the scope of this study but is also mTORC-regulated and subject to daily regulation (Ma *et al*, 2011; Ryzhikov *et al*, 2019). *In vivo*, daily regulation of mTORC activity arises primarily through growth factor signalling associated with daily feed/fast cycles (Crosby *et al*, 2019; Byles *et al*, 2021). The mechanisms facilitating cell-autonomous circadian mTORC activity rhythms are incompletely understood but may include Mg.ATP availability (Feeney *et al*, 2016a) and its direct regulation by PERIOD2 (Wu *et al*, 2019). This will be an important area for future work.

Increased translation will inevitably be associated with increased production of defective translation products, such as prematurely terminated or misfolded peptides that must be rapidly cleared by ubiquitin-proteasome system-mediated degradation (Dimitrova *et al*,

2009; Wang *et al*, 2013; Gandin & Topisirovic, 2014). Proteome-wide cycling ubiquitination sites have been recently described (Hansen *et al*, 2021); here we present evidence of cell-autonomous circadian rhythms of proteasome activity and rhythmic turnover for a greater proportion of the proteome than oscillates in abundance. Accordingly, temporal coordination was found for the synthesis of heteromeric protein complexes, in particular the ribosome, the most abundant protein complex in most mammalian cells. This highlights how, even though most mammalian proteins exhibit half-lives >24h and show little daily variation in abundance, the rate at which they are replaced can be subject to circadian regulation. This may be particularly beneficial for heteromeric complex assembly. Within the MMC fraction, we observed enrichment for specific biological functions at different times of the day, e.g., ribonucleoprotein assembly vs actin polymerisation. While bulk measurements showed clear coordination on the global scale, data from whole-cell and fractionated proteomics suggest that a combination of rhythmic synthesis, degradation, crowding and sequestration acts in concert to temporally organise rhythmic macromolecular biogenesis and assembly whilst minimising changes in overall proteome composition.

More insight into the relationship between temporal organisation and proteostasis can be gained by comparing our findings with other model systems. For example, we recently found chronic proteostasis imbalance in cells and tissues deficient for the *Cry1* and *Cry2* genes, without which circadian regulation of transcription does not persist. These cells exhibit increased proteotoxic stress as well as increased circadian variation in proteome composition compared with wild-type controls (Wong *et al*, 2022). Moreover, the temporal compartmentalisation of proteome renewal processes has a clear precedent in yeast, where metabolic oscillations arise as a direct consequence of TORC-dependent cycles of protein synthesis and sequestration that are critical for preventing deleterious protein aggregation (O'Neill *et al*, 2020). In light of similar findings in the alga *Ostreococcus tauri* (Kay *et al*, 2021; Feeney *et al*, 2016a), we speculate that promoting and minimising the energetic cost of proteostasis may be an evolutionarily conserved function of circadian and related biological rhythms.

Beyond testing two key predictions in mouse liver, a limitation is that this study was restricted to quiescent primary mouse fibroblasts. In our experience, fibroblasts are a particularly powerful and predictive model for fundamental principles of cellular circadian regulation (Hoyle *et al*, 2017). Clearly though, in future it will be necessary to extend our initial findings of protein turnover *in vivo* to fully validate that daily rhythms of protein turnover and proteome renewal occur under natural conditions (daily light/dark, feed/fast, rest/activity cycles). We predict that they will be observed across multiple mature tissues, with higher amplitude than cultured cells due to amplification of cell-intrinsic processes by daily systemic cues (hormonal and body temperature rhythms). We anticipate that the relative phases of synthesis and degradation rhythms will likely differ somewhat between tissues and physiological contexts, as recently found in growing muscle for example (Kelu *et al*, 2020).

Rhythms in transcription were not addressed in this study, but as discussed above, there is a well-established discrepancy between identities and phases of rhythmic proteins and their underlying transcript levels. Regulation at the translational level has been suggested to explain these differences, although ribosomal profiling studies have noted that on average there appears to be no delay between rhythmic transcript and nascent translation (Atger *et al*, 2015; Janich *et al*, 2015; Jang *et al*, 2015). We note, however, that ribosomal profiling reports on the level and position of ribosome-mRNA association, and so does not directly measure nascent protein production. Although a good correlate when comparing steady-state conditions, ribosome profiling also does not distinguish between active and stalled ribosomes, and does not reflect all the changes in protein synthesis that occur in dynamic cellular systems or upon perturbation that globally alter proteostasis (Liu *et al*, 2017). Upon finding evidence for global changes in protein synthesis and degradation throughout the day, the development of our pulsed SILAC method was crucial for allowing us direct insight into the regulation of protein abundance. Enabled by technological improvements in peptide detection accuracy and multiplexing, this is the first report of proteins tracked both across their lifetime (production) and across the circadian cycle. Moreover, our development of a simple pulse-labelling assay for nascent ribosome assembly likely has several applications beyond circadian research.

Finally, given the extensive links between proteome imbalance and many pathological states, daily regulation of protein metabolism has implications for health and disease. Circadian disruption is already strongly associated with impaired proteostasis, though causal mechanisms are poorly understood at this time (Bolitho *et al*, 2014; Musiek *et al*, 2018; Leng *et al*, 2019; Lipton *et al*, 2017; Wong *et al*, 2022). In this study we predicted and validated that daily turnover rhythms confer daily variation on the sensitivity of cells and tissues to a clinically relevant proteasome inhibitor. This highlights how preclinical models may help to accelerate the development of (chrono)therapies, that optimise treatment outcomes by leveraging understanding of the body's innate daily rhythms (Cederroth *et al*, 2019).

Methods

Cell culture and general timecourse structure

Fibroblasts originated from mice homozygous for PER2::LUCIFERASE (Yoo *et al*, 2004), isolated from lung tissue and were immortalised by serial passaging as described previously (Seluanov *et al*, 2010). For routine culture, cells were maintained at 37°C and 5% CO_2 in Gibco™ high glucose Dulbecco's Modified Eagle Medium (DMEM), supplemented with 100 units/ml penicillin and 100 µg/ml streptomycin, as well as 10% Hyclone™ III FetalClone™ bovine serum (GE Healthcare). When plated for experiments, cells were grown to confluence prior to the start of assaying, which ensures contact inhibition and elimination of cell division effects during the experiments (Hoyle *et al*, 2017; Ribatti, 2017).

For all the timecourse experiments, cells were subject to temperature entrainment, consisting of 12h:12h cycles of 32°C:37°C, for at least 4 days prior to the start of assaying, with media changes if required. Unless stated otherwise, the final medium change, containing 10% serum, occurred at the anticipated transition from 37°C to 32°C, as the cells were transferred to constant 37°C. This is denoted as experimental time t=0, or start of constant conditions. Sampling began at least 24h afterwards (i.e. t=24+), to avoid any transient effects of the last serum-containing medium change and temperature shift (Balsalobre *et al*, 1998; Buhr *et al*, 2010; Beale *et al*, 2023b). Parallel recording of PER2::LUCIFERASE activity were obtained using ALLIGATOR (Cairn Research) (Crosby *et al*, 2017), and luminescence quantified in Fiji/ImageJ v2.0 (Abramoff, 2007; Schindelin *et al*, 2012).

Cell lysis and protein quantification

For timecourse experiments requiring cell lysate collections, the procedure was based on the following. Cells were washed twice with PBS, and incubated with the indicated lysis buffers: normally either digitonin buffer (0.01% digitonin, 50 mM Tris pH 7.4, 5 mM EDTA, 150 mM NaCl) for 10 min on ice or urea/thiourea buffer for 20 min at room temperature (7 M urea, 2 M thiourea, 1% sodium deoxycholate, 20 mM Tris, 5 mM TCEP), both supplemented with protease and phosphatase inhibitor tablets (Roche, 4906845001 and 04693159001) added shortly beforehand. Cells were then scraped, and lysates transferred

587 to Eppendorf tubes, before sonication with Bioruptor sonicator (Diagenode) at 4°C, for 2-3
588 cycles 30 s on/30 s off. Lysates were then centrifuged at 14000 rpm for 5 min, and
589 supernatant either flash frozen in liquid nitrogen for future use, or taken directly for further
590 analysis. For determination of protein concentration, Pierce bicinchoninic acid assay (BCA)
591 (Smith *et al*, 1985) was performed in microplate format according to manufacturer's
592 instructions, with bovine serum albumin (BSA) protein standards diluted in the same lysis
593 buffer as experimental samples. Pierce 660 nm assay was performed instead of BCA when
594 samples contained thiourea.
595
596 ***^{35}S pulse-chase labelling***
597 All procedures for ^{35}S pulse-chase were optimised to avoid methionine starvation, serum-
598 containing media changes, and temperature perturbations, all of which could potentially
599 reset circadian rhythms and obscure any cell-autonomous regulation. Fibroblasts were
600 adapted to serum-free but otherwise complete medium starting from the last 4 days of
601 temperature entrainment. At each timepoint, the cells were pulsed with 0.1 mCi/ml ^{35}S-L-
602 methionine and ^{35}S-L-cysteine mix (EasyTag™ EXPRESS35S Protein Labeling Mix, Perkin
603 Elmer) in methionine- and cysteine-free DMEM for 15 min. For chase, the radiolabel-
604 containing media were replaced with standard DMEM supplemented with 2 mM (10x
605 normal concentration) of non-radiolabelled methionine and cysteine, and cells incubated for
606 1h. Throughout both pulse and chase the cells were maintained at 37°C. At the end of pulse
607 and chase periods, cells were washed with ice-cold PBS and lysed in digitonin buffer (0.01%
608 digitonin (Invitrogen), 50 mM Tris pH 7.4, 5 mM EDTA, 150 mM NaCl for 10 min on ice).
609 Lysates were run on NuPage™ Novex™ 4-12% Bis-Tris protein gels; the gels were then
610 stained with Coomassie SimplyBlue™ SafeStain (ThermoFisher). Gels were then dried at
611 80°C for 45 min and exposed overnight to a storage phosphor screen (GE Healthcare, BAS-IP
612 SR 2025), which was subsequently imaged with Typhoon FLA700 gel scanner and quantified
613 in Fiji/ImageJ.
614
615 ***Puromycin labelling***
616 Puromycin dihydrochloride, diluted in PBS, alone or in combination with BTZ, was added
617 directly to cells in culture medium, as 10x bolus to a final concentration of 1 µg/ml

puromycin and 1 µM BTZ. Labelling proceeded for 30 min at 37°C, after which cells were lysed in a urea/thiourea buffer and puromycin detected by Western blotting.

AHA incorporation

At each timepoint, while still maintaining cells at 37°C, complete DMEM medium was replaced with methionine-free DMEM supplemented with AHA in combination with methionine at 30:1 ratio (Bagert *et al*, 2014) – 1 mM AHA, 33 µM Met - and 1% dialysed FBS for 90 min. Cells were lysed in digitonin buffer (HEPES rather than Tris-buffered). AHA-containing proteins were conjugated to biotin by click chemistry, by adding appropriate reagents (Jena Bioscience) to the lysates, to final concentrations of 1 mM THPTA, 1 mM $CuSO_4$, 2 mM Na ascorbate, and 40 µM biotin alkyne, and incubating for 1h at room temperature. Biotinylated proteins were then detected by Western blotting.

Western blotting

Samples for denaturing polyacrylamide gel electrophoresis (SDS-PAGE) were prepared by diluting lysates with reduced NuPage™ LDS sample buffer and heating at 70°C for 10 min. Samples were run on NuPage™ Novex™ 4-12% Bis-Tris protein gels in MES buffer or on E-PAGE 8% 48-well gels (ThermoFisher). For native running conditions, NuPAGE Tris-Acetate 3% - 8% gels were used, with buffers as per manufacturer's instructions.

For Western blotting for puromycin and AHA incorporation measurement, chemiluminescence detection was used. Proteins were transferred from the gels to nitrocellulose membranes using an iBlot system (ThermoFisher). Membranes were stained by Ponceau as control for total protein loading, then washed, blocked, and incubated with primary antibody in the blocking buffer at 4°C overnight. Anti-puromycin antibody (PMY-2A4-2 from Developmental Studies Hybridoma bank, at 1:1000) was used with 5% milk in TBST blocking buffer, and an anti-mouse HRP-conjugated secondary antibody, while AHA-biotin was detected using Strep-HRP antibody (R-1098-1 from EpiGentek at 1:2000) in 1% BSA, 0.2% Triton X100 PBS blocking buffer, with additional 10% BSA blocking step before detection. Immobilon reagents (Millipore) were used to detect chemiluminescence. Images were analysed by densitometry in ImageLab v4.1 (BioRad).

650 For Western blotting of total and p-eIF2α, LICOR protocols and reagents were used. Briefly,
651 methanol-activated PVDF-FL (Immobilon) membranes were utilised for transfer, and dried
652 for 1h before blocking. After re-activation, membranes were blocked in Intercept TBS
653 buffer. Primary (AHO0802 from ThermoFisher, ab32157 from Abcam, both at 1:1000) and
654 secondary (IRDye 680RD and IRDye 800CW) antibodies were diluted in Intercept TBS buffer
655 with addition of 0.2% Tween-20. Fluorescence was detected and quantified in Odyssey® CLx
656 Imaging system.
657
658 ***Proteasome activity assays***
659 Cell-based ProteasomeGlo™ chymotrypsin-like and trypsin-like assays (Promega) were
660 performed according to manufacturer's instructions (Moravec *et al*, 2009) at multiple
661 circadian timepoints as indicated. Briefly, cells in 96-well plates and the assay reagent were
662 equilibrated to room temperature, before reagent addition, mixing, incubation for 10 min,
663 and luminescence measurement with Tecan Spark 10M plate reader, with integration time
664 of 1 s per well. For analysis, bioluminescence from negative control wells (containing only
665 culture medium and the assay reagent, but no cells) was subtracted from all the
666 experimental conditions.
667
668 ***Aggregation assays***
669 PROTEOSTAT® Aggresome Detection kit (Enzo Life Sciences) was used for detection of
670 protein aggregates (Shen *et al*, 2011). Cells in 96-well plates were treated with MG132 (as
671 indicated in the figure legends), added as 10x bolus diluted in serum-free DMEM to the pre-
672 existing culture media, and gently titurated, to avoid cellular rhythms resetting. Cells were
673 permeabilised and stained simultaneously with PROTEOSTAT® dye and Hoechst 33342, as
674 per kit manufacturer's manual. Total fluorescence in blue and red channels, and
675 representative images of individual wells were acquired using Tecan Spark Cyto plate
676 reader.
677
678 ***Viability assays***
679 PrestoBlue™ High Sensitivity reagent (ThermoFisher), a resazurin-based dye, was used to
680 measure cellular viability (Boncler *et al*, 2014; Xu *et al*, 2015). Cells in 96-well plates were
681 treated with drugs or DMSO (vehicle) controls, as indicated in figure legends, added as 10x

bolus diluted in serum-free DMEM on top of existing culture media. For drug washout in the timecourse experiments, cell medium was replaced with 1% serum DMEM, to allow recovery for 18 h. The assay was then performed in line with manufacturer's guidelines: following PrestoBlue reagent addition and incubation at 37°C for 20 min, fluorescence was measured in a Tecan Spark 10M plate reader, with excitation at 550 nm and emission at 600 nm.

General statistics

Statistical tests were performed using GraphPad Prism (v8 and v9) and R v4, and are indicated in figure legends. *P* values are either reported in figures directly, or annotated with asterisks: * $p \leq 0.05$; ** $p \leq 0.01$, *** $p \leq 0.001$; **** $p \leq 0.0001$, *ns* not significant, $p>0.05$. Number of replicates are reported as *n* or *N* (for technical and biological, respectively) in the figures; error bars represent standard error (SEM) unless stated otherwise. In cases where comparison of fits was performed, determining whether the data are better described by a straight line or a cosine wave with circadian period, the following equation was used for the latter:

$$y = (mx + c) + ae^{kx} \cos\frac{2\pi x - r}{p}$$

Where *m* is the baseline, *c* is the offset from 0 in y-axis, *a* is the amplitude, *k* is the damping rate, *r* is the phase, and *p* is the period, which was fixed at either 24 hours or 25 hours depending on the parallel PER2::LUC recording period.

Proteomics data collection and analysis

Cell culture and sample collection for pSILAC-TMT

For pSILAC-TMT experiments, mouse lung fibroblasts were cultured in 10% dialysed FBS (dFBS). SILAC labelling was conducted in DMEM supplemented with 1% dialysed FBS and heavy-labelled amino acids instead of their light analogues, specifically 84 mg/L $^{13}C_6{}^{15}N_4$ L-Arginine and 146 mg/L $^{13}C_6{}^{15}N_2$ L-Lysine (Ong *et al*, 2002). In the first timecourse pSILAC experiment, sets of cells were labelled for 6h, every 6h over two days, and total cell lysates were extracted in urea/thiourea-based buffer (n=1 per timepoint). In the second timecourse

712 experiments, labelling was done for 1.5h, every 6h over two days in duplicates, and
713 fractionation performed as described below. For the booster channel, a fully-heavy labelled
714 sample was used, where cells were cultured in DMEM with heavy amino acids for 5
715 passages (3-4 w) but otherwise processed in the same way as the timecourse samples.
716 Fractionation was based on LOPIT-DC protocol (Geladaki *et al*, 2019). Two 15cm dishes per
717 sample were used, cells were scraped in ice-cold PBS, centrifuged, and then lysed on ice by
718 resuspension in a mild buffer (0.25 M sucrose, 10 mM HEPES pH 7.4, 2 mM EDTA, 2 mM
719 magnesium acetate, protease inhibitors) and passaged through a Dounce homogeniser.
720 Lysates were moved to thick-wall ultracentrifuge tubes (Beckman 343778 11mm/34mm)
721 and centrifuged at 79 000 *g* for 43 min to pellet membranes and organelles. Supernatant
722 was then centrifuged again at 120 000 *g* for 45 min. Resulting pellet was resuspended in 8 M
723 urea 20 mM Tris buffer, and processed for mass spectrometry analysis.
724
725 ***Mass spectrometry analysis***
726 *Protein digestion*

727 Protein samples were reduced with 5 mM DTT at 56°C for 30 min and alkylated with 10 mM
728 iodoacetamide in the dark at room temperature for 30 min. The samples were then diluted
729 to 3M urea and digested with Lys-C (Promega) for 4 h at 25°C. Next, the samples were
730 further diluted to 1.6 M urea and were digested with trypsin (Promega) overnight, at 30°C.
731 After digestion, an equal volume of ethyl acetate was added and acidified with formic acid
732 (FA) to a final concentration of 0.5%, mixed by shaking for 3 min and centrifuged at 15700 *g*
733 for 2 min. The top organic layer was removed and the bottom aqueous phase was desalted
734 using home-made C18 stage tips (3M Empore) filled with porous R3 resin (Applied
735 Biosystems). The stage tips were equilibrated with 80% acetonitrile (MeCN) and 0.5% FA,
736 followed by 0.5% FA. Bound peptides were eluted with 30-80% MeCN and 0.5% FA and
737 lyophilized.
738
739 *Tandem mass tag (TMT) labelling*

740 Dried peptide mixtures (50 µg) from each condition were resuspended in 24 µl of 200 mM
741 HEPES, pH 8.5. 12 µl (300 µg) TMTpro 16plex or 18plex reagent (ThermoFisher)
742 reconstituted according to manufacturer's instructions was added and incubated at room

743 temperature for 1 h. The labelling reaction was then terminated by incubation with 2.2 µl
744 5% hydroxylamine for 30 min. The labelled peptides were pooled into a single sample and
745 desalted using the same stage tips method as above.

746

747 *Off-line high pH reverse-phase peptides fractionation*

748 200 µg of the labelled peptides were separated on an off-line, high pressure liquid
749 chromatography (HPLC). The experiment was carried out using XBridge BEH130 C18, 5 µm,
750 2.1 x 150 mm column (Waters), connected to an Ultimate 3000 analytical HPLC (Dionex).
751 Peptides were separated with a gradient of 1-90% buffer A and B (A: 5% MeCN, 10 mM
752 ammonium bicarbonate, pH8; B: MeCN, 10 mM ammonium bicarbonate, pH8, [9:1]) in 60
753 min at a flow rate of 250 µl/min. A total of 54 fractions were collected, which were then
754 combined into 18 fractions and lyophilized. Dried peptides were resuspended in 1% MeCN
755 and 0.5% FA, and desalted using C18 stage tips, ready for mass spectrometry analysis.

756

757 *Mass spectra acquisition*

758 The fractionated peptides were analysed by LC-MS/MS using a fully automated Ultimate
759 3000 RSLC nano System (ThermoFisher) fitted with a 100 µm x 2 cm PepMap100 C18 nano
760 trap column and a 75 µm×25 cm, nanoEase M/Z HSS C18 T3 column (Waters). Peptides were
761 separated by a non-linear gradient of 120 min, 6-38% buffer B (80% MeCN, 0.1% FA). Eluted
762 peptides were introduced directly via a nanoFlex ion source into an Orbitrap Eclipse mass
763 spectrometer (ThermoFisher). Data were acquired using FAIMS-Pro device, running
764 MS3_RTS analysis, switching between two compensation voltages (CV) of -50 and -70 V.

765 MS1 spectra were acquired using the following settings: R = 120K; mass range = 400-1400
766 m/z; AGC target = 4e5; MaxIT = 50 ms. Charge states 2-5 were included and dynamic
767 exclusion was set at 60 s. MS2 analysis were carried out with collision induced dissociation
768 (CID) activation, ion trap detection, AGC = 1e4, MaxIT = 35 ms, CE = 34%, and isolation
769 window = 0.7 m/z. RTS-SPS-MS3 was set up to search Uniport *Mus musculus* proteome
770 (2021), with fixed modifications cysteine carbamidomethylation and TMTpro at the peptide
771 N-terminal. TMTpro K, Arg10 (R +10.008), TMTpro K+K8 (K +312.221) and methionine
772 oxidation were set as dynamic modifications. Missed cleavages were allowed, and maximum

773 variable modifications was set at 3. In MS3 scans, the selected precursors were fragmented
774 by high-collision dissociation (HCD), and analysed using the orbitrap with the following
775 settings: isolation window = 0.7 m/z, NCE = 55, orbitrap resolution = 50K, scan range = 110-
776 500 m/z, MaxIT = 200ms, and AGC = 1e5.

777

778 *Raw MS data processing*

779 The acquired 18 raw files from LC-MS/MS were each split into two individual spectra, one
780 with CV = -50V and one with CV = -70V, total 36 files, using FreeStyle software
781 (ThermoFisher). These files were then processed using MaxQuant (Cox & Mann, 2008) with
782 the integrated Andromeda search engine (v1.6.17.0). MS/MS spectra were quantified with
783 reporter ion MS3 from TMTpro experiments and searched against UniProt *Mus musculus*
784 Reviewed (Nov 2020) Fasta databases. Carbamidomethylation of cysteines was set as a fixed
785 modification, while methionine oxidation, N-terminal acetylation, Arg10 and Lys8 were set
786 as variable modifications.

787

788 ***Data analysis***

789 After the MaxQuant search, all subsequent proteomics data processing and analysis was
790 performed in R (v3.6.1 and v4.1.2) with R Studio v1.2. The custom scripts are available via a
791 github repository, at https://github.com/estere-sei/circadian-pSILAC

792

793 Peptide level information from MaxQuant (evidence.txt output file) was used as a starting
794 point. Contaminants and reverse hits were removed. Peptides were classified according to
795 their labelling state: those that had at least one heavy arginine (Arg10) or lysine (Lys8) were
796 classified as “heavy”, and the rest were classified as “light”. Entries for peptides with
797 identical sequences in the same labelling state were grouped together (i.e. their reporter
798 ion intensities across the 16 TMT channels were summed up), including peptides with other
799 modifications such as methionine oxidation. Peptides with missing values were excluded.
800 Total heavy label incorporation was quantified as overall proportion of summed intensities
801 of heavy peptides over total summed intensities per TMT channel. Sample loading
802 normalisation was performed, applying a scaling factor to equalise total summed intensity
803 across TMT channels.

Peptides were filtered to leave only those that were detected in both heavy and light form. Peptide intensities belonging to the same leading razor protein accession were summed up to get total protein abundance value, while the sum of heavy peptides only for each protein represented the amount of synthesis. The ratio of heavy to total protein intensity averaged across the 8 timepoints was used to estimate relative turnover.

Several methods were used to assess the likelihood of significant circadian change over time in proteins' total abundance and synthesis, including Rhythmicity Analysis Incorporating Non-parametric Methods (RAIN) (Thaben & Westermark, 2014) and ANOVA. With RAIN, the data were tested for rhythms with period length of 24 h. For ANOVA, the data were log-transformed, and two days of sampling were treated as replicates. Oscillation phase was taken from RAIN outputs, and represented circadian time of the peak of oscillation, where time 0 is equivalent to the peak of PER2::LUC from parallel recordings. The extent of change over time is expressed as fold-change, taking average ratio of peak to trough intensity values across the two days of sampling.

For protein complex membership analysis, a list was taken from Ori *et al.*, 2016 which combined CORUM, COMPLEAT and manually annotated complexes and their subunits (Ori *et al*, 2016; Giurgiu *et al*, 2019; Vinayagam *et al*, 2013). Ensembl gene identifiers were converted from human to mouse by g:Profiler g:Orth tool (Raudvere *et al*, 2019), and matched with detected proteins. To asses variability of complex turnover, an analysis similar to one in Mathieson *et al.*, 2018 was performed: standard deviation of the average relative turnover was calculated between proteins belonging to each detected complex, taking only complexes with more than 4 subunits, and compared to a dataset of the same size and structure but with proteins chosen randomly from all detected proteins (i.e. same number of complexes with same number of subunits as in annotated data but "subunits" chosen by random sampling).

For gene ontology functional enrichment analysis, GOrilla tool was used (Eden *et al*, 2009), comparing target protein list with all detected proteins as background, and setting FDR q-value cutoff at 0.05. REVIGO (0.4) was used to remove redundant terms. For analysis of

836 protein-protein interactions, STRING web app was used (Szklarczyk *et al*, 2021), filtering for
837 high-confidence physical interactions, and looking for enrichment against the background of
838 detected proteins.
839
840 ***Mouse tissue experiments***
841 All animal work was licensed by the Home Office under the Animals (Scientific Procedures)
842 Act 1986, with Local Ethical Review by the Medical Research Council and the University of
843 Cambridge, UK. Throughout the experiments, wild-type C57 mice were housed in 12:12 h
844 light:dark conditions.
845
846 For *in vivo* turnover measurements, mice received i.p. injections of either 40 µmol/kg
847 puromycin (Ravi *et al*, 2020, 2018; Schmidt *et al*, 2009), or 40 µmol/kg puromycin in
848 combination with 2.5 mg/kg BTZ (Apex Bio). Both solutions were sterile-filtered in PBS with
849 1% DMSO. Animals were culled 45 min after, in the same order as injected, and livers
850 collected and flash frozen in liquid nitrogen. The procedure was performed twice on the
851 same day, 1 h after the transition from dark to light (ZT1), and 1 h after the transition from
852 light to dark (ZT13). Four age-matched male mice were used per condition.
853
854 For *in vivo* response to proteotoxic stress measurements, mice received i.p. injections of 2.5
855 mg/kg BTZ (Apex Bio) or vehicle control (1% DMSO in PBS, sterile-filtered). Animals were
856 culled 5 h after, in the same order as injected, and livers collected and flash frozen in liquid
857 nitrogen. Injections were performed twice on the same day, 1 h after the transition from
858 dark to light (ZT1), and 1 h after the transition from light to dark (ZT13). 6 age-matched male
859 mice were used per condition.
860
861 Tissues were homogenised in urea/thiourea lysis buffers in Precellys 24 Tissue Homogeniser
862 (Bertin Instruments), using CK14 ceramic beads, for 3 x 15 s at 5000 rpm with 30 s breaks.
863 Lysates were then cleared by centrifugation at 14000 rpm for 5 min, followed by protein
864 sample preparation and Western blotting as previously described.
865
866 ***Edmondson assay for nascent rRNA labelling***
867

At each timepoint, whilst maintaining fibroblasts at constant 37°C, 200 µM isotopically heavy uridine ($^{15}N_{2-}$, Cambridge Isotope Laboratories) was spiked into media for 6 h to label nascently transcribed RNA. After labelling, cells were harvested by trypsinisation, and pellets immediately flash frozen and stored at −70 °C.

For ribosome extraction, each cell pellet was resuspended in 200 µl of lysis buffer (40 mM HEPES·KOH (pH 7.5), 75 mM KOAc·HOAc, 5 mM $Mg(OAc)_2$·HOAc, 1 mM $CaCl_2$, 10 µM $Zn(OAc)_2$·HOAc, 2 mM spermidine, 5 mM dithiothreitol, 1% v/v Triton X-100) and sonicated at 4 °C for 5 min (30 s on; 30 s off). To each lysate, 2 µl of micrococcal nuclease (Nuclease S7, Roche) was added and the lysates were incubated at 25 °C for 18 min using a thermal cycler (Techne-Prime, Cole-Parmer). Processed lysates were immediately flash-frozen in liquid nitrogen and stored at −70 °C.

Ribosomal RNA samples and cell pellets for total RNA extraction were resuspended in 'RLT Buffer' and RNA extracted and purified using the RNeasy Mini kit (Qiagen, 74004) according to the manufacturer's instructions, including the on-column DNase-treatment (Qiagen, 79254). RNA was then further purified via an overnight ethanol precipitation at −20 °C, and RNA pellets resuspended in pre-heated 'Physiological Buffer' (50 mM HEPES·KOH (pH 7.5), 100 mM KOAc·HOAc, 20 mM $Mg(OAc)_2$·HOAc). RNA was then degraded into single nucleotides by overnight room temperature incubation with micrococcal nuclease (Nuclease S7, Roche) supplemented with 1 mM $CaCl_2$. The digestion reaction was then terminated by flash-freezing, and samples stored at -70°C.

LC-MS analysis of UMP and heavy UMP in RNA lysates

10 µl of RNA lysate was diluted in 40 µl of 10 mM ammonium acetate and transferred to a 96 well skirted PCR plate (Starlab International, Hamburg, Germany) and covered with a silicone sealing mat (Axymat, Salt Lake City, Utah, USA) prior to mixed mode LC-MS analysis using an ACE Excel C18-PFP (pentafluorophenyl) column (150 × 2.1 mm, 2.0 µm, Hichrom, Reading, Berkshire, UK). Mobile phase A consisted of water with 0.1% formic acid with 10 mM ammonium formate and mobile phase B was acetonitrile with 0.1% formic acid. For gradient elution mobile phase B was held at 0% for 1.6 min. followed by a linear gradient to

30% B over 4.0 minutes, a further increase to 90% over 1 min. and a hold at 90% B for 1 min. with re-equilibration for 1.5 minutes giving a total run time of 6.5 minutes. The flow rate was 0.5 mL/min and the injection volume was 3 µL. The needle wash used was 1:1 water: acetonitrile.

For MS analysis using the Q Exactive Plus (ThermoFisher Scientific, Hemel Hempstead, Hertfordshire, UK) a full scan of 60-900 m/z was used at a resolution of 70,000 ppm in positive ion mode. The source parameters were as follows: an auxiliary gas temperature of 450ºC, a capillary temperature of 275 ºC, an ion spray voltage of 3.5 kV and a sheath gas, auxiliary gas and sweep gas of 55, 15 and 3 arbitrary units respectively.

Samples were analysed using Xcalibur (Thermofisher, Version 4.2) and processed and integrated using the Qual Browser and Quan Browser tools within Xcalibur to target specific analytes. Data were expressed as area ratios between areas of extracted ion chromatograms of UMP (m/z 325.0431) against 15N2 UMP (m/z 327.0372) and all identifications of compounds were carried out using reference of the accurate mass and verified using standards purchased from Sigma Aldrich.

Acknowledgements

We thank all members of O'Neill lab, Rachel Edgar, Manu Hegde and Szymon Juszkiewicz for valuable feedback and discussions, as well as Kathryn Lilley and Holger Kramer for advice on proteomics. We also thank biomedical technical staff at Medical Research Council (MRC) Ares facility and LMB facilities for assistance. NMR was supported by the Medical Research Council (MR/S022023/1). JON was supported by the Medical Research Council (MC_UP_1201/4).

Author contributions

ES and JON designed the study, analysed the data and wrote the manuscript with assistance from JM and ADB; SYP-C and JW performed mass spectrometry; NMR, AZ and JON performed mouse studies; ES, AE, AZ and NRJ performed cell experiments; DCSW, JM and ADB provided further experimental assistance and valuable intellectual contributions. All authors commented on the manuscript.

References

Abramoff M (2007) ImageJ as an Image Processing Tool and Library. *Microscopy and Microanalysis* 13

Adegoke OAJ, Beatty BE, Kimball SR & Wing SS (2019) Interactions of the super complexes: When mTORC1 meets the proteasome. *The International Journal of Biochemistry & Cell Biology* 117: 105638

Albornoz N, Bustamante H, Soza A & Burgos P (2019) Cellular Responses to Proteasome Inhibition: Molecular Mechanisms and Beyond. *International Journal of Molecular Sciences* 20: 3379

An H & Harper JW (2020) Ribosome Abundance Control Via the Ubiquitin–Proteasome System and Autophagy. *J Mol Biol* 432: 170–184

Andreani TS, Itoh TQ, Yildirim E, Hwangbo D-S & Allada R (2015) Genetics of Circadian Rhythms. *Sleep Medicine Clinics* 10: 413–421

Atger F, Gobet C, Marquis J, Martin E, Wang J, Weger B, Lefebvre G, Descombes P, Naef F & Gachon F (2015) Circadian and feeding rhythms differentially affect rhythmic mRNA transcription and translation in mouse liver. *Proc National Acad Sci* 112: E6579--E6588

Atger F, Mauvoisin D, Weger B, Gobet C & Gachon F (2017) Regulation of Mammalian Physiology by Interconnected Circadian and Feeding Rhythms. *Frontiers in Endocrinology* 8

Balsalobre A, Damiola F & Schibler U (1998) A Serum Shock Induces Circadian Gene Expression in Mammalian Tissue Culture Cells. *Cell* 93: 929–937

Beale AD, Hayter EA, Crosby P, Valekunja UK, Edgar RS, Chesham JE, Maywood ES, Labeed FH, Reddy AB, Wright KP, *et al* (2023a) Mechanisms and physiological function of daily haemoglobin oxidation rhythms in red blood cells. *EMBO J*: e114164

Beale AD, Rzechorzek NM, Mihut A, Zeng A, Smyllie NJ, Pilorz V, Richardson R, Bertlesen MF, James NR, Fazal SV, *et al* (2023b) Thermosensitivity of translation underlies the mammalian nocturnal-diurnal switch. *bioRxiv*: 2023.06.22.546020

Ben-Sahra I & Manning BD (2017) mTORC1 signaling and the metabolic control of cell growth. *Current Opinion in Cell Biology* 45: 72–82

Blobel G & Potter VR (1967) Studies on free and membrane-bound ribosomes in rat liver I. Distribution as related to total cellular RNA. *J Mol Biol* 26: 279–292

966 Bolitho SJ, Naismith SL, Rajaratnam SMW, Grunstein RR, Hodges JR, Terpening Z, Rogers N &
967 Lewis SJG (2014) Disturbances in melatonin secretion and circadian sleep–wake
968 regulation in Parkinson disease. *Sleep Medicine* 15: 342–347

969 Boncler M, Różalski M, Krajewska U, Podsędek A & Watala C (2014) Comparison of
970 PrestoBlue and MTT assays of cellular viability in the assessment of anti-proliferative
971 effects of plant extracts on human endothelial cells. *Journal of Pharmacological and*
972 *Toxicological Methods* 69: 9–16

973 Brooks TG, Manjrekar A, Mrcˇela A & Grant GR (2023) Meta-analysis of Diurnal
974 Transcriptomics in Mouse Liver Reveals Low Repeatability of Rhythm Analyses. *J Biol*
975 *Rhythm*: 7487304231179600

976 Buchan JR & Parker R (2009) Eukaryotic Stress Granules: The Ins and Outs of Translation.
977 *Molecular Cell* 36: 932–941

978 Buhr ED, Yoo S-H & Takahashi JS (2010) Temperature as a Universal Resetting Cue for
979 Mammalian Circadian Oscillators. *Science* 330: 379–385

980 Buttgereit F & Brand MD (1995) A hierarchy of ATP-consuming processes in mammalian
981 cells. *Biochemical Journal* 312: 163–167

982 Byles V, Cormerais Y, Kalafut K, Barrera V, Hallett JEH, Sui SH, Asara JM, Adams CM, Hoxhaj
983 G, Ben-Sahra I, *et al* (2021) Hepatic mTORC1 signaling activates ATF4 as part of its
984 metabolic response to feeding and insulin. *Mol Metab* 53: 101309

985 Cao R (2018) mTOR Signaling, Translational Control, and the Circadian Clock. *Frontiers in*
986 *Genetics* 9

987 Cederroth CR, Albrecht U, Bass J, Brown SA, Dyhrfjeld-Johnsen J, Gachon F, Green CB,
988 Hastings MH, Helfrich-Förster C, Hogenesch JB, *et al* (2019) Medicine in the Fourth
989 Dimension. *Cell Metabolism* 30: 238–250

990 Cox J & Mann M (2008) MaxQuant enables high peptide identification rates, individualized
991 p.p.b.-range mass accuracies and proteome-wide protein quantification. *Nature*
992 *Biotechnology* 26: 1367–1372

993 Cox KH & Takahashi JS (2019) Circadian clock genes and the transcriptional architecture of
994 the clock mechanism. *Journal of Molecular Endocrinology* 63: R93–R102

995 Crosby P, Hamnett R, Putker M, Hoyle NP, Reed M, Karam CJ, Maywood ES, Stangherlin A,
996 Chesham JE, Hayter EA, *et al* (2019) Insulin/IGF-1 Drives PERIOD Synthesis to Entrain
997 Circadian Rhythms with Feeding Time. *Cell* 177: 896-909.e20

998 Crosby P, Hoyle NP & O'Neill JS (2017) Flexible Measurement of Bioluminescent Reporters
999 Using an Automated Longitudinal Luciferase Imaging Gas- and Temperature-optimized
1000 Recorder (ALLIGATOR). *J Vis Exp*

1001 Dantuma NP & Lindsten K (2010) Stressing the ubiquitin-proteasome system. *Cardiovascular*
1002 *Research* 85: 263–271

1003 Delarue M, Brittingham GP, Pfeffer S, Surovtsev IV, Pinglay S, Kennedy KJ, Schaffer M,
1004 Gutierrez JI, Sang D, Poterewicz G, *et al* (2018) mTORC1 Controls Phase Separation and
1005 the Biophysical Properties of the Cytoplasm by Tuning Crowding. *Cell* 174: 338-349.e20

1006 Deshaies RJ (2014) Proteotoxic crisis, the ubiquitin-proteasome system, and cancer therapy.
1007 *BMC Biology* 12

1008 Desvergne A, Ugarte N, Radjei S, Gareil M, Petropoulos I & Friguet B (2016) Circadian
1009 modulation of proteasome activity and accumulation of oxidized protein in human
1010 embryonic kidney HEK 293 cells and primary dermal fibroblasts. *Free Radical Biology and*
1011 *Medicine* 94: 195–207

1012 Dibner C, Schibler U & Albrecht U (2010) The Mammalian Circadian Timing System:
1013 Organization and Coordination of Central and Peripheral Clocks. *Annu Rev Physiol* 72:
1014 517–549

1015 Dieterich DC, Link AJ, Graumann J, Tirrell DA & Schuman EM (2006) Selective identification
1016 of newly synthesized proteins in mammalian cells using bioorthogonal noncanonical
1017 amino acid tagging (BONCAT). *Proc Natl Acad Sci* 103: 9482–9487

1018 Dimitrova LN, Kuroha K, Tatematsu T & Inada T (2009) Nascent Peptide-dependent
1019 Translation Arrest Leads to Not4p-mediated Protein Degradation by the Proteasome.
1020 *Journal of Biological Chemistry* 284: 10343–10352

1021 Doherty MK, Hammond DE, Clague MJ, Gaskell SJ & Beynon RJ (2009) Turnover of the
1022 Human Proteome: Determination of Protein Intracellular Stability by Dynamic SILAC.
1023 *Journal of Proteome Research* 8: 104–112

1024 Eden E, Navon R, Steinfeld I, Lipson D & Yakhini Z (2009) GOrilla: a tool for discovery and
1025 visualization of enriched GO terms in ranked gene lists. *BMC Bioinformatics* 10

1026 Feeney KA, Hansen LL, Putker M, Olivares-Yañez C, Day J, Eades LJ, Larrondo LF, Hoyle NP,
1027 O'Neill JS & Ooijen G van (2016a) Daily magnesium fluxes regulate cellular timekeeping
1028 and energy balance. *Nature* 532: 375–379

1029 Feeney KA, Putker M, Brancaccio M & O'Neill JS (2016b) In-depth Characterization of Firefly
1030 Luciferase as a Reporter of Circadian Gene Expression in Mammalian Cells. *J Biol Rhythm*
1031 31: 540–550

1032 Gandin V & Topisirovic I (2014) Co-translational mechanisms of quality control of newly
1033 synthesized polypeptides. *Translation* 2: e28109

1034 Geladaki A, Britovšek NK, Breckels LM, Smith TS, Vennard OL, Mulvey CM, Crook OM, Gatto
1035 L & Lilley KS (2019) Combining LOPIT with differential ultracentrifugation for high-
1036 resolution spatial proteomics. *Nature Communications* 10

1037 Gerber A, Esnault C, Aubert G, Treisman R, Pralong F & Schibler U (2013) Blood-Borne
1038 Circadian Signal Stimulates Daily Oscillations in Actin Dynamics and SRF Activity. *Cell* 152:
1039 492–503

1040 Giurgiu M, Reinhard J, Brauner B, Dunger-Kaltenbach I, Fobo G, Frishman G, Montrone C &
1041 Ruepp A (2019) CORUM: the comprehensive resource of mammalian protein
1042 complexes—2019. *Nucleic Acids Research* 47: D559–D563

1043 Hansen FM, Tanzer MC, Brüning F, Bludau I, Stafford C, Schulman BA, Robles MS, Karayel O
1044 & Mann M (2021) Data-independent acquisition method for ubiquitinome analysis
1045 reveals regulation of circadian biology. *Nat Commun* 12: 254

1046 Harper JW & Bennett EJ (2016) Proteome complexity and the forces that drive proteome
1047 imbalance. *Nature* 537: 328–338

1048 Hipp MS, Kasturi P & Hartl FU (2019) The proteostasis network and its decline in ageing.
1049 *Nature Reviews Molecular Cell Biology* 20: 421–435

1050 Hoyle NP, Seinkmane E, Putker M, Feeney KA, Krogager TP, Chesham JE, Bray LK, Thomas
1051 JM, Dunn K, Blaikley J, *et al* (2017) Circadian actin dynamics drive rhythmic fibroblast
1052 mobilization during wound healing. *Sci Transl Med* 9: eaal2774

1053 Hughes ME, Abruzzi KC, Allada R, Anafi R, Arpat AB, Asher G, Baldi P, Bekker C de, Bell-
1054 Pedersen D, Blau J, *et al* (2017) Guidelines for Genome-Scale Analysis of Biological
1055 Rhythms. *J Biol Rhythm* 32: 380–393

1056 Jang C, Lahens NF, Hogenesch JB & Sehgal A (2015) Ribosome profiling reveals an important
1057 role for translational control in circadian gene expression. *Genome Res* 25: 1836–1847

1058 Janich P, Arpat AB, Castelo-Szekely V, Lopes M & Gatfield D (2015) Ribosome profiling
1059 reveals the rhythmic liver translatome and circadian clock regulation by upstream open
1060 reading frames. *Genome Res* 25: 1848–1859

1061 Jiang H-Y & Wek RC (2005) Phosphorylation of the α-Subunit of the Eukaryotic Initiation
1062 Factor-2 (eIF2α) Reduces Protein Synthesis and Enhances Apoptosis in Response to
1063 Proteasome Inhibition. *Journal of Biological Chemistry* 280: 14189–14202

1064 Jouffe C, Cretenet G, Symul L, Martin E, Atger F, Naef F & Gachon F (2013) The Circadian
1065 Clock Coordinates Ribosome Biogenesis. *Plos Biol* 11: e1001455

1066 Juszkiewicz S & Hegde RS (2018) Quality Control of Orphaned Proteins. *Molecular Cell* 71:
1067 443–457

1068 Karki S, Castillo K, Ding Z, Kerr O, Lamb TM, Wu C, Sachs MS & Bell-Pedersen D (2020)
1069 Circadian clock control of eIF2α phosphorylation is necessary for rhythmic translation
1070 initiation. *Proc National Acad Sci* 117: 10935–10945

1071 Kay H, Grünewald E, Feord HK, Gil S, Peak-Chew SY, Stangherlin A, O'Neill JS & Ooijen G van
1072 (2021) Deep-coverage spatiotemporal proteome of the picoeukaryote Ostreococcus tauri
1073 reveals differential effects of environmental and endogenous 24-hour rhythms. *Commun*
1074 *Biology* 4: 1147

1075 Kelu JJ, Pipalia TG & Hughes SM (2020) Circadian regulation of muscle growth independent
1076 of locomotor activity. *Proceedings of the National Academy of Sciences* 117: 31208–
1077 31218

1078 Klann K, Tascher G & Münch C (2020) Functional Translatome Proteomics Reveal Converging
1079 and Dose-Dependent Regulation by mTORC1 and eIF2α. *Mol Cell* 77: 913-925.e4

1080 Labbadia J & Morimoto RI (2015) The Biology of Proteostasis in Aging and Disease. *Annual*
1081 *Review of Biochemistry* 84: 435–464

1082 Lacsina JR, Marks OA, Liu X, Reid DW, Jagannathan S & Nicchitta CV (2012) Premature
1083 Translational Termination Products Are Rapidly Degraded Substrates for MHC Class I
1084 Presentation. *PLoS ONE* 7: e51968

1085 Lane N & Martin W (2010) The energetics of genome complexity. *Nature* 467: 929–934

1086 Leng Y, Musiek ES, Hu K, Cappuccio FP & Yaffe K (2019) Association between circadian
1087 rhythms and neurodegenerative diseases. *The Lancet Neurology* 18: 307–318

1088 Lipton JO, Boyle LM, Yuan ED, Hochstrasser KJ, Chifamba FF, Nathan A, Tsai PT, Davis F &
1089 Sahin M (2017) Aberrant Proteostasis of BMAL1 Underlies Circadian Abnormalities in a
1090 Paradigmatic mTOR-opathy. *Cell Reports* 20: 868–880

1091 Lipton JO, Yuan ED, Boyle LM, Ebrahimi-Fakhari D, Kwiatkowski E, Nathan A, Güttler T, Davis
1092 F, Asara JM & Sahin M (2015) The Circadian Protein BMAL1 Regulates Translation in
1093 Response to S6K1-Mediated Phosphorylation. *Cell* 161: 1138–1151

1094 Liu T-Y, Huang HH, Wheeler D, Xu Y, Wells JA, Song YS & Wiita AP (2017) Time-Resolved
1095 Proteomics Extends Ribosome Profiling-Based Measurements of Protein Synthesis
1096 Dynamics. *Cell Systems* 4: 636-644.e9

1097 Ma D, Panda S & Lin JD (2011) Temporal orchestration of circadian autophagy rhythm by
1098 C/EBPβ: C/EBPβ regulates circadian autophagy rhythm. *EMBO J* 30: 4642–4651

1099 Ma Y & Yates JR (2018) Proteomics and pulse azidohomoalanine labeling of newly
1100 synthesized proteins: what are the potential applications? *Expert Rev Proteom* 15: 545–
1101 554

1102 Malcolm M, Saad L, Penazzi LG & Garbarino-Pico E (2019) Processing Bodies Oscillate in
1103 Neuro 2A Cells. *Frontiers in Cellular Neuroscience* 13

1104 Manasanch EE & Orlowski RZ (2017) Proteasome inhibitors in cancer therapy. *Nature*
1105 *Reviews Clinical Oncology* 14: 417–433

1106 Marshall RS & Vierstra RD (2019) Dynamic Regulation of the 26S Proteasome: From
1107 Synthesis to Degradation. *Front Mol Biosci* 6: 40

1108 Mathieson T, Franken H, Kosinski J, Kurzawa N, Zinn N, Sweetman G, Poeckel D, Ratnu VS,
1109 Schramm M, Becher I, *et al* (2018) Systematic analysis of protein turnover in primary
1110 cells. *Nat Commun* 9: 1--10

1111 Mauvoisin D & Gachon F (2020) Proteomics in Circadian Biology. *J Mol Biol* 432: 3565–3577

1112 Mauvoisin D, Wang J, Jouffe C, Martin E, Atger F, Waridel P, Quadroni M, Gachon F & Naef F
1113 (2014) Circadian clock-dependent and -independent rhythmic proteomes implement
1114 distinct diurnal functions in mouse liver. *Proceedings of the National Academy of*
1115 *Sciences* 111: 167–172

1116 Mei W, Jiang Z, Chen Y, Chen L, Sancar A & Jiang Y (2021) Genome-wide circadian rhythm
1117 detection methods: systematic evaluations and practical guidelines. *Brief Bioinform* 22:
1118 bbaa135

1119 Musiek ES, Bhimasani M, Zangrilli MA, Morris JC, Holtzman DM & Ju Y-ES (2018) Circadian
1120 Rest-Activity Pattern Changes in Aging and Preclinical Alzheimer Disease. *JAMA*
1121 *Neurology* 75: 582

1122 O'Neill JS, Hoyle NP, Robertson JB, Edgar RS, Beale AD, Peak-Chew SY, Day J, Costa ASH,
1123 Frezza C & Causton HC (2020) Eukaryotic cell biology is temporally coordinated to
1124 support the energetic demands of protein homeostasis. *Nat Commun* 11: 4706

1125 Ong S-E, Blagoev B, Kratchmarova I, Kristensen DB, Steen H, Pandey A & Mann M (2002)
1126 Stable Isotope Labeling by Amino Acids in Cell Culture, SILAC, as a Simple and Accurate
1127 Approach to Expression Proteomics. *Molecular & Cellular Proteomics* 1: 376–386

1128 Ori A, Iskar M, Buczak K, Kastritis P, Parca L, Andrés-Pons A, Singer S, Bork P & Beck M
1129 (2016) Spatiotemporal variation of mammalian protein complex stoichiometries.
1130 *Genome Biology* 17

1131 Palazzo AF & Lee ES (2015) Non-coding RNA: what is functional and what is junk? *Front*
1132 *Genet* 6: 2

1133 Pathak SS, Liu D, Li T, Zavalia N de, Zhu L, Li J, Karthikeyan R, Alain T, Liu AC, Storch K-F, *et al*
1134 (2019) The eIF2α Kinase GCN2 Modulates Period and Rhythmicity of the Circadian Clock
1135 by Translational Control of Atf4. *Neuron* 104: 724-735.e6

1136 Price JC, Guan S, Burlingame A, Prusiner SB & Ghaemmaghami S (2010) Analysis of
1137 proteome dynamics in the mouse brain. *Proceedings of the National Academy of Sciences*
1138 107: 14508–14513

1139 Putker M, Crosby P, Feeney KA, Hoyle NP, Costa ASH, Gaude E, Frezza C & O'Neill JS (2018)
1140 Mammalian Circadian Period, But Not Phase and Amplitude, Is Robust Against Redox and
1141 Metabolic Perturbations. *Antioxid Redox Sign* 28: 507–520

1142 Ramanathan C, Kathale ND, Liu D, Lee C, Freeman DA, Hogenesch JB, Cao R & Liu AC (2018)
1143 mTOR signaling regulates central and peripheral circadian clock function. *Plos Genet* 14:
1144 e1007369

1145 Raudvere U, Kolberg L, Kuzmin I, Arak T, Adler P, Peterson H & Vilo J (2019) g:Profiler: a web
1146 server for functional enrichment analysis and conversions of gene lists (2019 update).
1147 *Nucleic Acids Research* 47: W191–W198

1148 Ravi V, Jain A, Ahamed F, Fathma N, Desingu PA & Sundaresan NR (2018) Systematic
1149 evaluation of the adaptability of the non-radioactive SUnSET assay to measure cardiac
1150 protein synthesis. *Scientific Reports* 8

1151 Ravi V, Jain A, Mishra S & Sundaresan NR (2020) Measuring Protein Synthesis in Cultured
1152 Cells and Mouse Tissues Using the Non-radioactive SUnSET Assay. *Current Protocols in*
1153 *Molecular Biology* 133

1154 Reddy AB, Karp NA, Maywood ES, Sage EA, Deery M, O'Neill JS, Wong GKY, Chesham J, Odell
1155 M, Lilley KS, *et al* (2006) Circadian Orchestration of the Hepatic Proteome. *Current*
1156 *Biology* 16: 1107–1115

1157 Ribatti D (2017) A revisited concept: Contact inhibition of growth. From cell biology to
1158 malignancy. *Experimental Cell Research* 359: 17–19

1159 Riggs CL, Kedersha N, Ivanov P & Anderson P (2020) Mammalian stress granules and P
1160 bodies at a glance. *Journal of Cell Science* 133

1161 Robles MS, Cox J & Mann M (2014) In-Vivo Quantitative Proteomics Reveals a Key
1162 Contribution of Post-Transcriptional Mechanisms to the Circadian Regulation of Liver
1163 Metabolism. *PLoS Genetics* 10: e1004047

1164 Ross AB, Langer JD & Jovanovic M (2021) Proteome Turnover in the Spotlight: Approaches,
1165 Applications, and Perspectives. *Molecular & Cellular Proteomics* 20: 100016

1166 Ryzhikov M, Ehlers A, Steinberg D, Xie W, Oberlander E, Brown S, Gilmore PE, Townsend RR,
1167 Lane WS, Dolinay T, *et al* (2019) Diurnal Rhythms Spatially and Temporally Organize
1168 Autophagy. *Cell Reports* 26: 1880-1892.e6

1169 Rzechorzek NM, Connick P, Patani R, Selvaraj BT & Chandran S (2015) Hypothermic
1170 Preconditioning of Human Cortical Neurons Requires Proteostatic Priming. *EBioMedicine*
1171 2: 528–535

1172 Santiago AM, Gonçalves DL & Morano KA (2020) Mechanisms of sensing and response to
1173 proteotoxic stress. *Experimental Cell Research* 395: 112240

1174 Schindelin J, Arganda-Carreras I, Frise E, Kaynig V, Longair M, Pietzsch T, Preibisch S, Rueden
1175 C, Saalfeld S, Schmid B, *et al* (2012) Fiji: an open-source platform for biological-image
1176 analysis. *Nature Methods* 9: 676–682

1177 Schmidt EK, Clavarino G, Ceppi M & Pierre P (2009) SUnSET, a nonradioactive method to
1178 monitor protein synthesis. *Nature Methods* 6: 275–277

1179 Schubert U, Antón LC, Gibbs J, Norbury CC, Yewdell JW & Bennink JR (2000) Rapid
1180 degradation of a large fraction of newly synthesized proteins by proteasomes. *Nature*
1181 404: 770–774

1182 Schwanhäusser B, Busse D, Li N, Dittmar G, Schuchhardt J, Wolf J, Chen W & Selbach M
1183 (2011) Global quantification of mammalian gene expression control. *Nature* 473: 337–
1184 342

1185 Seluanov A, Vaidya A & Gorbunova V (2010) Establishing Primary Adult Fibroblast Cultures
1186 From Rodents. *J Vis Exp*

1187 Shen D, Coleman J, Chan E, Nicholson TP, Dai L, Sheppard PW & Patton WF (2011) Novel
1188 Cell- and Tissue-Based Assays for Detecting Misfolded and Aggregated Protein
1189 Accumulation Within Aggresomes and Inclusion Bodies. *Cell Biochemistry and Biophysics*
1190 60: 173–185

1191 Sinturel F, Gerber A, Mauvoisin D, Wang J, Gatfield D, Stubblefield JJ, Green CB, Gachon F &
1192 Schibler U (2017) Diurnal Oscillations in Liver Mass and Cell Size Accompany Ribosome
1193 Assembly Cycles. *Cell* 169: 651-663.e14

1194 Smith PK, Krohn RI, Hermanson GT, Mallia AK, Gartner FH, Provenzano MD, Fujimoto EK,
1195 Goeke NM, Olson BJ & Klenk DC (1985) Measurement of protein using bicinchoninic acid.
1196 *Analytical Biochemistry* 150: 76–85

1197 Stangherlin A, Seinkmane E & O'Neill JS (2021a) Understanding circadian regulation of
1198 mammalian cell function, protein homeostasis, and metabolism. *Curr Opin Syst Biology*
1199 28: 100391

1200 Stangherlin A, Watson JL, Wong DCS, Barbiero S, Zeng A, Seinkmane E, Chew SP, Beale AD,
1201 Hayter EA, Guna A, *et al* (2021b) Compensatory ion transport buffers daily protein
1202 rhythms to regulate osmotic balance and cellular physiology. *Nat Commun* 12: 6035

1203 Szeto J, Kaniuk NA, Canadien V, Nisman R, Mizushima N, Yoshimori T, Bazett-Jones DP &
1204 Brumell JH (2006) ALIS are Stress-Induced Protein Storage Compartments for Substrates
1205 of the Proteasome and Autophagy. *Autophagy* 2: 189–199

1206 Szklarczyk D, Gable AL, Nastou KC, Lyon D, Kirsch R, Pyysalo S, Doncheva NT, Legeay M, Fang
1207 T, Bork P, *et al* (2021) The STRING database in 2021: customizable protein–protein
1208 networks, and functional characterization of user-uploaded gene/measurement sets.
1209 *Nucleic Acids Research* 49: D605–D612

1210 Taggart JC, Zauber H, Selbach M, Li G-W & McShane E (2020) Keeping the Proportions of
1211 Protein Complex Components in Check. *Cell Systems* 10: 125–132

1212 Thaben PF & Westermark PO (2014) Detecting Rhythms in Time Series with RAIN. *Journal of*
1213 *Biological Rhythms* 29: 391–400

1214 Valvezan AJ & Manning BD (2019) Molecular logic of mTORC1 signalling as a metabolic
1215 rheostat. *Nat Metab* 1: 321–333

1216 Vinayagam A, Hu Y, Kulkarni M, Roesel C, Sopko R, Mohr SE & Perrimon N (2013) Protein
1217 Complex–Based Analysis Framework for High-Throughput Data Sets. *Science Signaling* 6

1218 Wagner PM, Prucca CG, Velazquez FN, Alderete LGS, Caputto BL & Guido ME (2021)
1219 Temporal regulation of tumor growth in nocturnal mammals: In vivo studies and
1220 chemotherapeutical potential. *The FASEB Journal* 35

1221 Wang F, Durfee LA & Huibregtse JM (2013) A Cotranslational Ubiquitination Pathway for
1222 Quality Control of Misfolded Proteins. *Mol Cell* 50: 368–378

1223 Wang R, Jiang X, Bao P, Qin M & Xu J (2019) Circadian control of stress granules by
1224 oscillating EIF2α. *Cell Death Dis* 10

1225 Welsh DK, Yoo S-H, Liu AC, Takahashi JS & Kay SA (2004) Bioluminescence Imaging of
1226 Individual Fibroblasts Reveals Persistent, Independently Phased Circadian Rhythms of
1227 Clock Gene Expression. *Curr Biol* 14: 2289–2295

1228 Wheatley D, Giddings M & Inglis M (1980) Kinetics of degradation of short- and long-lived
1229 proteins in cultured mammalian cells. *Cell Biology International Reports* 4: 1081–1090

1230 Wolff S, Weissman JS & Dillin A (2014) Differential Scales of Protein Quality Control. *Cell*
1231 157: 52–64

1232 Wong DCS, Seinkmane E, Zeng A, Stangherlin A, Rzechorzek NM, Beale AD, Day J, Reed M,
1233 Peak-Chew SY, Styles CT, *et al* (2022) CRYPTOCHROMES promote daily protein
1234 homeostasis. *Embo J* 41: e2021108883

1235 Wu R, Dang F, Li P, Wang P, Xu Q, Liu Z, Li Y, Wu Y, Chen Y & Liu Y (2019) The Circadian
1236 Protein Period2 Suppresses mTORC1 Activity via Recruiting Tsc1 to mTORC1 Complex.
1237 *Cell Metab* 29: 653-667.e6

1238 Xu M, McCanna DJ & Sivak JG (2015) Use of the viability reagent PrestoBlue in comparison
1239 with alamarBlue and MTT to assess the viability of human corneal epithelial cells. *Journal*
1240 *of Pharmacological and Toxicological Methods* 71: 1–7

1241 Yoo S-H, Yamazaki S, Lowrey PL, Shimomura K, Ko CH, Buhr ED, Siepka SM, Hong H-K, Oh
1242 WJ, Yoo OJ, *et al* (2004) PERIOD2::LUCIFERASE real-time reporting of circadian dynamics
1243 reveals persistent circadian oscillations in mouse peripheral tissues. *P Natl Acad Sci Usa*
1244 101: 5339–5346

Zhang R, Lahens NF, Ballance HI, Hughes ME & Hogenesch JB (2014) A circadian gene expression atlas in mammals: Implications for biology and medicine. *Proc National Acad Sci* 111: 16219–16224

Zhang X, Linder S & Bazzaro M (2020) Drug Development Targeting the Ubiquitin–Proteasome System (UPS) for the Treatment of Human Cancers. *Cancers* 12: 902

Zhuang Y, Li Z, Xiong S, Sun C, Li B, Wu SA, Lyu J, Shi X, Yang L, Chen Y, *et al* (2023) Circadian clocks are modulated by compartmentalized oscillating translation. *Cell* 186: 3245-3260.e23

Figure legends

Figure 1.

A A representative phosphor screen exposure of SDS-PAGE gel showing ^{35}S-Met/Cys incorporation in 15 min pulse (P) and 1 h chase (C) samples at different circadian times in mouse lung fibroblasts lysed with digitonin buffer.
B Quantification of radiolabel signal in pulse and chase at the different timepoints, normalised to protein content (by Coomassie stain) in four replicates shown in Fig S1A. Statistics: two-way ANOVA with Dunnett's multiple comparison test, comparing T24 to other timepoints. On the right, the inferred degradation within 1h of chase is plotted, calculated as 100%*(1-Chase/Pulse). Statistics: one-way ANOVA with Dunnett's multiple comparison test, comparing T24 to other timepoints.
C Chymotrypsin-like, trypsin-like, and caspase-like proteasome activities, measured by ProteasomeGlo cell-based assays, at different circadian times as indicated. Statistics: damped cosine wave fit compared with straight line (null hypothesis) by extra sum-of-squares F test, the statistically preferred fit is plotted and p-value displayed. Parallel PER2::LUC bioluminescence recording from replicate cell cultures (mean +/- SEM, every 30 min) is shown below, acting as phase marker.
D Schematic representation of the optimised puromycin incorporation assay. Puromycin (Puro) is incorporated into nascent peptide chains during translation elongation. A subset of these gets degraded by the proteasome within the 30 min labelling timeframe, resulting in a measure of "net" translation. In the presence of bortezomib (BTZ), the proteasome is inhibited, so the peptides that would have been degraded are still present and can be detected. Thus, all nascently translated peptide chains can be detected. Degradation can be inferred from comparing the two conditions, and allows estimation of both translation and degradation in a single assay.
E Quantification of total protein, protein synthesis and protein turnover from a puromycin incorporation timecourse, where at each of the 12 timepoints Puro ± BTZ was added directly to cell media, and cells lysed 30 min afterwards in digitonin buffer. Puromycin incorporation was assessed by Western blotting, and total protein from a parallel Ponceau Red stain. Change in degradation was calculated from fitted data of puromycin incorporation, relative to mean degradation level. Statistics: damped cosine wave fit compared with straight line (null hypothesis) by extra sum-of-squares F test, the

statistically preferred fit is plotted and p-value displayed. Parallel PER2::LUC bioluminescence recording from replicate cell cultures (mean +/- SEM, every 30 min) is shown below, acting as phase marker (example phase comparison is shown as dashed line).

F Puromycin incorporation *in vivo*: mice received an i.p. injection of puromycin with or without BTZ at ZT1 or ZT13 (note: zeitgeber = 'time-giver' and indicates hours since initial lights on). Livers were harvested 40 min afterwards and extracted with urea/thiourea buffer. Representative anti-puromycin Western blot is shown, and quantification is shown on the right, normalised for protein loading as assessed by Coomassie staining. Statistics: two-way ANOVA with Sidak's multiple comparisons test. Four mice were used per condition, but in some cases one of the four injections were not successful i.e. no puromycin labelling was observed and so no quantification could be performed (full data in Fig S2B).

Figure 2.

A Schematic of circadian pulsed SILAC-TMT experiment design. In a set of entrained fibroblasts, at each circadian timepoint "light" media (DMEM with standard L-Arg and L-Lys) is switched for "heavy" (DMEM with $^{13}C_6{}^{15}N_4$ L-Arg and $^{13}C_6{}^{15}N_2$ L-Lys), and cells lysed after 6h. Lysates are then digested, labelled with tandem mass tags (TMT), mixed and analysed by mass spectrometry. Data are presented aligned with the midpoint of the labelling window.

B Parallel bioluminescence recording of PER2::LUC, acting as phase marker, overlayed with SILAC labelling windows that were used for the timecourse.

C Representative examples of proteins (taken from Supplemental Table 1) changing rhythmically or staying constant in their total abundance (left) or synthesis (right), as measured in the pSILAC-TMT timecourse and rhythmicity defined by RAIN p<0.05. R-epresentative of rhythmic abundance and synthesis: Akap12; representative of arrhythmic abundance and synthesis: Dnmt1; representative of rhythmic abundance but arrhythmic synthesis: Rnf170; and representative of arrhythmic abundance but rhythmic synthesis: Nup107.

D Probability density distribution of fold-change between peak and trough for proteins rhythmic in synthesis and in total abundance, representing the extent of change over time in these two sets. Statistics: Mann-Whitney test, $p < 0.0001$.

E Comparison of rhythmicity between individual proteins' synthesis and total abundance. Statistically, significant change over time was assessed by two algorithms, RAIN and ANOVA, with p<0.05 taken as rhythmicity threshold. (Top) Percentages of detected proteins falling under the four rhythmicity categories by the two algorithms are displayed; (Bottom) Venn diagrams of proteins significant for rhythms in synthesis and/or abundance. Degradation rhythms can account for cases of proteins with rhythms in synthesis but not abundance, or *vice versa*. Overall, 6264 proteins were detected; out of those at least one heavy peptide was detected for 2528 proteins (the set used for the analysis).

F Phase distribution of proteins rhythmic (with threshold RAIN p<0.05) in both synthesis and total abundance, as well as their circadian phase difference. Gene ontology functional enrichment was tested for by GOrilla tool, in each phase separately or

together, against the background of all detected proteins, and no terms were significant below the corrected p-value (FDR q-value) 0.05 cutoff. Phase 0 is set as the peak of PER2::LUC.

G Phase distribution of proteins rhythmic (with threshold RAIN p<0.05) in their total abundance and in their synthesis. Phase 0 is set as the peak of PER2::LUC.

Figure 3.

A Schematic of circadian pulsed SILAC-TMT with extra fractionation step. In a set of entrained fibroblasts, at each circadian timepoint "light" media (DMEM with standard L-Arg and L-Lys) is switched for "heavy" (DMEM with $^{13}C_6{}^{15}N_4$ L-Arg and $^{13}C_6{}^{15}N_2$ L-Lys), and cells collected after 1.5h. Samples were then subjected to sequential ultracentrifugation, a method adjusted from Geladaki *et al.* 2019 LOPIT-DC protocol. The fraction enriched for macromolecular protein complexes (MMC fraction) was labelled with tandem mass tags (TMT), mixed and analysed by mass spectrometry.

B Parallel bioluminescence recording of PER2::LUC, acting as phase marker, overlayed with SILAC labelling windows that were used for the timecourse.

C Comparison of percentage of detected proteins that are considered rhythmic (p<0.05) in their synthesis by the two algorithms used, between the whole-cell pSILAC experiment, presented in Fig 2, and the experiment focused on complexes, presented in this figure.

D Probability density distribution of fold-change between peak and trough for proteins rhythmic in synthesis and in total abundance, representing the extent of change over time in these two sets. Statistics: Mann-Whitney test.

E Comparison of rhythmicity between individual proteins' synthesis and total abundance. Statistically, significant change over time was assessed by two algorithms, RAIN and ANOVA, with p<0.05 taken as rhythmicity threshold. Percentages of detected proteins falling under the four rhythmicity categories by the two algorithms are displayed. Overall, 6577 proteins were detected; out of those at least one heavy peptide was detected for 2302 proteins (the set used for the analysis).

F Coordinated turnover of proteins belonging to complexes: for four selected complexes, their annotated subunits (according to a compilation of CORUM, COMPLEAT and manual annotations) were averaged in terms of their fold-change over time (x-axis), and relative turnover (proportion of heavy to total peptide intensity averaged across 8 timepoints, y axis). All proteins are displayed in the background in grey. Normalised heavy abundance, i.e. synthesis, of these proteins over time is shown on heatmaps on the right.

G Proteins rhythmic (RAIN p<0.05) in their synthesis were analysed using STRING interaction database, filtering for high-confidence, physical interactions. Proteins with rhythmic synthesis in the complex fraction had an interconnected protein-protein interaction network, with high average node degree and significant enrichment in interactions over all detected proteins in that experiment, whereas for proteins with rhythmic synthesis in the whole-cell experiment (Fig 2) this was not the case.

H Fibroblasts were pulsed with AHA for 1.5h at the indicated timepoints, and AHA incorporation into protein complexes and other higher molecular weight species under native conditions, using biotin as click substrate and streptavidin-HRP for detection after non-denaturing gel electrophoresis. Signal was quantified and normalised to total

protein content as measured by SyproRuby (middle), and Ponceau stain of the native PAGE membrane (bottom) shows molecular weight of the loaded species. Statistics: damped cosine wave fit (plotted) preferred over straight line, extra sum-of-squares F test p-value displayed.

Figure 4.

A Phase distribution of proteins rhythmic (RAIN p<0.05) in their total abundance and in their synthesis in the MMC fraction. Gene ontology functional enrichment for biological processes was performed using GOrilla tool, with proteins at each phase compared against all detected proteins in this experiment, and FDR q-value (multiple comparisons adjusted p-value) threshold of 0.05. For phase "0/24", top significant non-overlapping terms are presented, alongside their significance and fold-enrichment values. In phase "18", terms associated with actin were enriched (q<0.05), e.g. "actin filament bundle assembly" (8.85-fold enrichment).
B Example proteins peaking at phase "0/24", belonging to terms associated with ribonucleoprotein complex assembly and stress granule assembly. Plotted are their abundance and synthesis in the MMC fraction as well as at whole-cell level (measured independently).
C Example proteins peaking at phase "18", associated with actin assembly. Plotted are their abundance and synthesis in the MMC fraction as well as at whole-cell level.

Figure 5

A Schematic of Edmondson assay for nascent rRNA labelling. In a set of entrained fibroblasts, at each circadian timepoint, 200 μM of heavy ($^{15}N_2$)-uridine is spiked into media for 6hr to metabolically label all nascent RNA prior to collecting cells. Total RNA or rRNA derived from assembled ribosomal complexes is extracted from cell pellets before treatment with micrococcal nuclease to completely digest RNA to free nucleotides monophosphates. The abundance of heavy and light uridine monophosphate (UMP) is then quantified by mass spectrometry.
B Circadian regulation of ribosome turnover detected by Edmondson assay. (Top) Total UMP abundance for total cellular RNA and rRNA in assembled ribosomes. (Middle) Heavy UMP reports RNA synthesised in the preceding 6 hours, expressed as a percentage of total cellular UMP and UMP that was incorporated within assembled ribosomes, respectively. Note that heavy UMP was first corrected for natural abundance detected in unlabelled fibroblasts. (Bottom) Parallel PER2::LUC bioluminescence recording, conducted under the same experimental and timecourse conditions. Statistics: damped cosine wave fit compared with straight line (null hypothesis) by extra sum-of-squares F test, the statistically preferred fit is plotted and p-value displayed.

Figure 6.

A (Left) Two sets of fibroblast lysates were collected every 4 h for 3 days, one untreated control and one treated with 20 μM MG132 proteasomal inhibitor for 4 h before each collection. Fold-change increase in relative phosphorylation of eIF2α (i.e. (p-eIF2α/total)$_{MG132}$/(p-eIF2α/total)$_{control}$) at each timepoint is plotted. MG132 is expected to induce increase in phosphorylation of eIF2α but the extent of the induction differs. Statistics: damped cosine wave fit (plotted) preferred over straight line, extra sum-of-squares F test p-value displayed. (Right) Parallel PER2::LUC bioluminescence recording, conducted under the same experimental and timecourse conditions as experiments in (A), (B) and (C).

B Cells were treated with 20 μM MG132 for 24h starting at indicated timepoints, and aggregation relative to untreated samples measured by Proteastat aggresome kit. MG132 is expected to induce aggregation but the extent of the induction differs. Statistics: One-way ANOVA $p<0.0001$, stars and colours represent Dunnett's multiple comparison of neighbouring timepoints. The difference between T24 & T48 as well as between T36 & T60 was not statistically significant.

C At 8 timepoints throughout 2 days, fibroblasts were treated with 2.5 μM proteasomal inhibitor bortezomib (BTZ), 25 μM translation inhibitor cycloheximide (CHX), or vehicle control; after 6 h, the drugs were washed out, allowing cells to recover for further 18 h. Cellular viability after the treatments, as measured by PrestoBlue High Sensitivity assay, is expressed as a proportion of control (vehicle-treated) cells at each timepoint. Statistics: damped cosine wave fit compared with straight line (null hypothesis) by extra sum-of-squares F test, the statistically preferred fit is plotted & p-value displayed.

D Time-of-day bortezomib (BTZ) effect *in vivo*: mice received an i.p. injection of BTZ or vehicle control (VEH) at ZT1 or ZT13, and livers were harvested 5h after the treatment. Representative Western blot is shown, blots, probed for total (green) and S51-phopshorylated (red) eIF2α.

E Quantification of relative phosphorylation levels of eIF2α from experiment in (D). Statistics: repeated measures two-way ANOVA with Sidak's multiple comparisons test

F Fold-change increase in phosphorylation of eIF2α upon bortezomib injection, quantified from (E). Statistics: paired t-test.

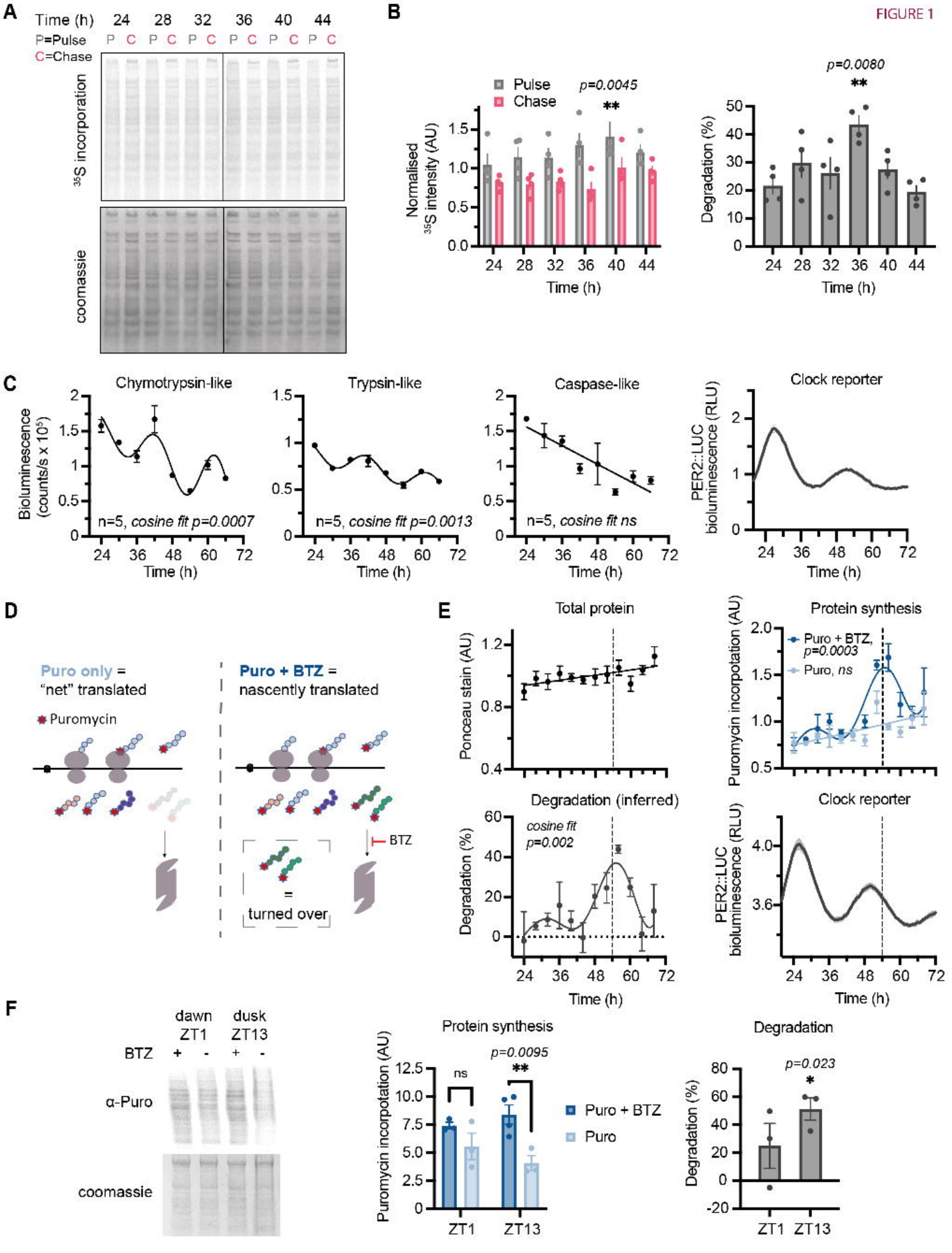
A
Time (h) 24 28 32 36 40 44
P=Pulse
C=Chase
P C P C P C P C P C P C
35S incorporation
coomassie
B
Pulse
Chase
p=0.0045
**
Normalised 35S intensity (AU)
Time (h)
p=0.0080
**
Degradation (%)
Time (h)
C
Chymotrypsin-like
Bioluminescence (counts/s x 10^5)
n=5, cosine fit p=0.0007
Time (h)
Trypsin-like
n=5, cosine fit p=0.0013
Time (h)
Caspase-like
n=5, cosine fit ns
Time (h)
Clock reporter
PER2::LUC bioluminescence (RLU)
Time (h)
D
Puro only = "net" translated
Puromycin
Puro + BTZ = nascently translated
BTZ
=
turned over
E
Total protein
Ponceau stain (AU)
Protein synthesis
Puromycin incorporation (AU)
Puro + BTZ, p=0.0003
Puro, ns
Degradation (inferred)
Degradation (%)
cosine fit
p=0.002
Time (h)
Clock reporter
PER2::LUC bioluminescence (RLU)
Time (h)
F
dawn ZT1
dusk ZT13
BTZ + - + -
α-Puro
coomassie
Protein synthesis
Puromycin incorporation (AU)
ns
p=0.0095
**
Puro + BTZ
Puro
ZT1
ZT13
Degradation
Degradation (%)
p=0.023
*
ZT1
ZT13

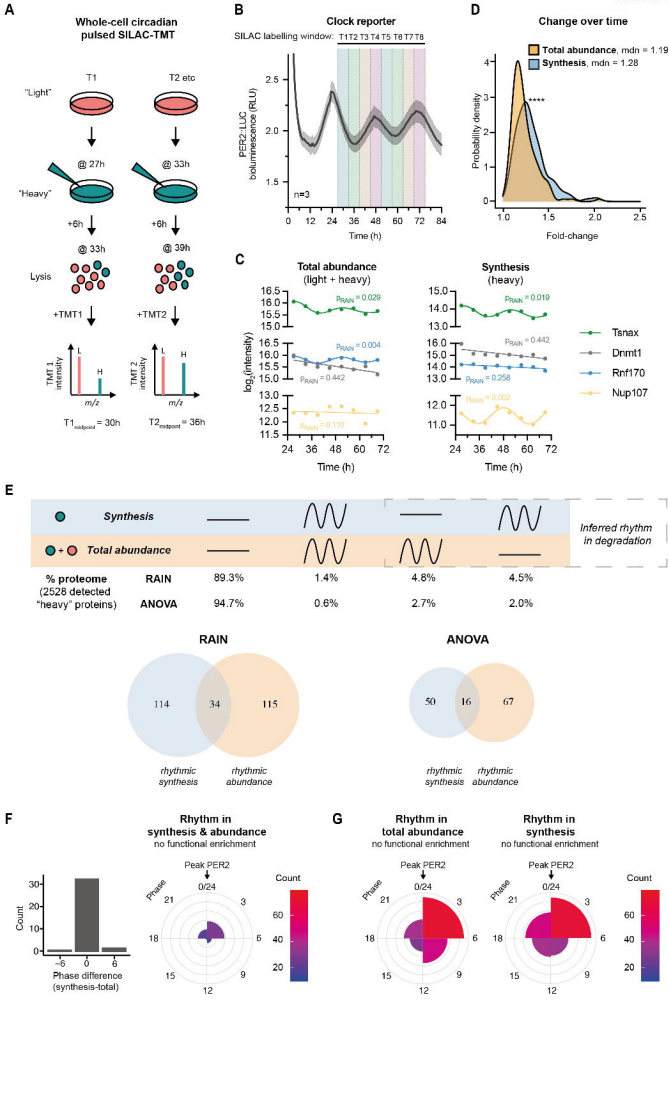
A
Whole-cell circadian pulsed SILAC-TMT
T1
T2 etc
"Light"
@ 27h
@ 33h
"Heavy"
+6h
+6h
@ 33h
@ 39h
Lysis
+TMT1
+TMT2
TMT 1 intensity
TMT 2 intensity
L
H
m/z
T1midpoint = 30h
T2midpoint = 36h
B
Clock reporter
SILAC labelling window: T1 T2 T3 T4 T5 T6 T7 T8
PER2::LUC bioluminescence (RLU)
n=3
Time (h)
D
Change over time
Total abundance, mdn = 1.19
Synthesis, mdn = 1.28
****
Probability density
Fold-change
C
Total abundance (light + heavy)
Synthesis (heavy)
log2(intensity)
PRAIN = 0.029
PRAIN = 0.004
PRAIN = 0.442
PRAIN = 0.110
PRAIN = 0.019
PRAIN = 0.442
PRAIN = 0.258
PRAIN = 0.002
Time (h)
Tsnax
Dnmt1
Rnf170
Nup107
E
Synthesis
Total abundance
Inferred rhythm in degradation
% proteome (2528 detected "heavy" proteins)
RAIN
ANOVA
89.3%
1.4%
4.8%
4.5%
94.7%
0.6%
2.7%
2.0%
RAIN
114
34
115
rhythmic synthesis
rhythmic abundance
ANOVA
50
16
67
rhythmic synthesis
rhythmic abundance
F
Rhythm in synthesis & abundance
no functional enrichment
Count
Phase difference (synthesis-total)
Peak PER2
0/24
Phase
G
Rhythm in total abundance
no functional enrichment
Rhythm in synthesis
no functional enrichment

FIGURE 3

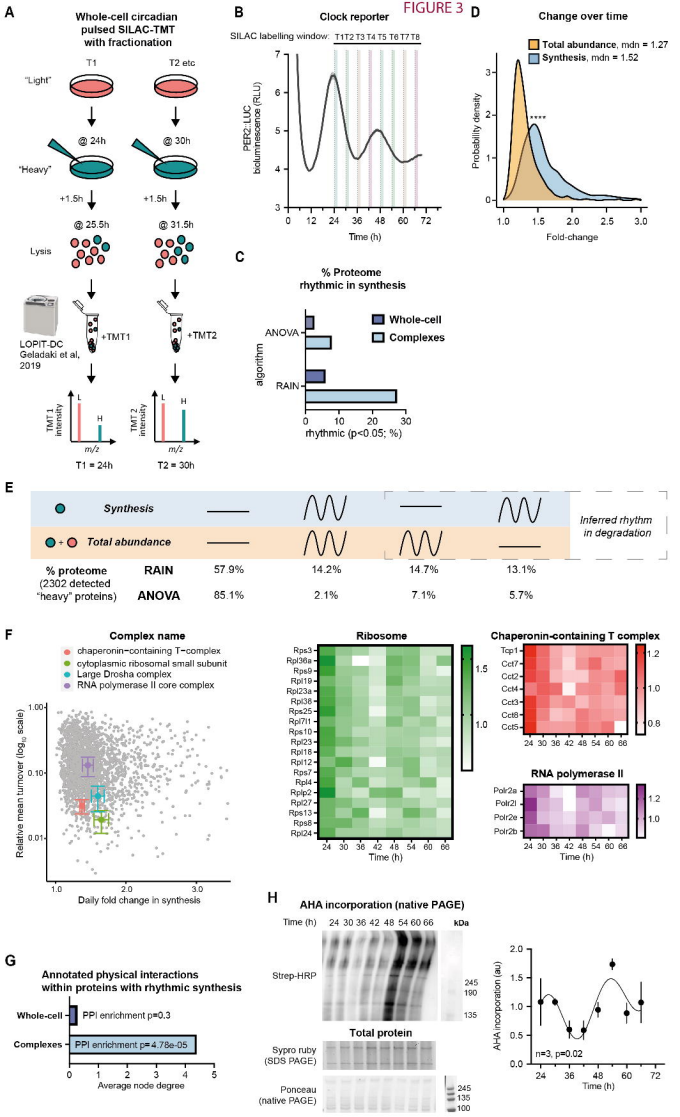
A
Whole-cell circadian pulsed SILAC-TMT with fractionation
T1
T2 etc
"Light"
@ 24h
@ 30h
"Heavy"
+1.5h
+1.5h
@ 25.5h
@ 31.5h
Lysis
LOPIT-DC Geladaki et al, 2019
+TMT1
+TMT2
TMT 1 intensity
TMT 2 intensity
L
H
m/z
T1 = 24h
T2 = 30h
B
Clock reporter
SILAC labelling window:
T1 T2 T3 T4 T5 T6 T7 T8
PER2::LUC bioluminescence (RLU)
Time (h)
C
% Proteome rhythmic in synthesis
Whole-cell
Complexes
ANOVA
RAIN
algorithm
rhythmic (p<0.05; %)
D
Change over time
Total abundance, mdn = 1.27
Synthesis, mdn = 1.52
****
Probability density
Fold-change
E
Synthesis
Total abundance
Inferred rhythm in degradation
% proteome (2302 detected "heavy" proteins)
RAIN
ANOVA
57.9%
85.1%
14.2%
2.1%
14.7%
7.1%
13.1%
5.7%
F
Complex name
chaperonin−containing T−complex
cytoplasmic ribosomal small subunit
Large Drosha complex
RNA polymerase II core complex
Relative mean turnover (log10 scale)
Daily fold change in synthesis
Ribosome
Rps3
Rpl36a
Rps6
Rpl19
Rpl23a
Rpl36
Rps25
Rpl7l1
Rps10
Rpl23
Rpl15
Rpl12
Rps7
Rpl4
Rplp2
Rpl27
Rps13
Rps8
Rpl24
Time (h)
Chaperonin-containing T complex
Tcp1
Cct7
Ccl2
Cct4
Cct3
Cct8
Cct5
RNA polymerase II
Polr2a
Polr2l
Polr2e
Polr2b
G
Annotated physical interactions within proteins with rhythmic synthesis
Whole-cell
Complexes
PPI enrichment p=0.3
PPI enrichment p=4.78e-05
Average node degree
H
AHA incorporation (native PAGE)
Time (h)
kDa
Strep-HRP
Total protein
Sypro ruby (SDS PAGE)
Ponceau (native PAGE)
AHA incorporation (au)
n=3, p=0.02
Time (h)

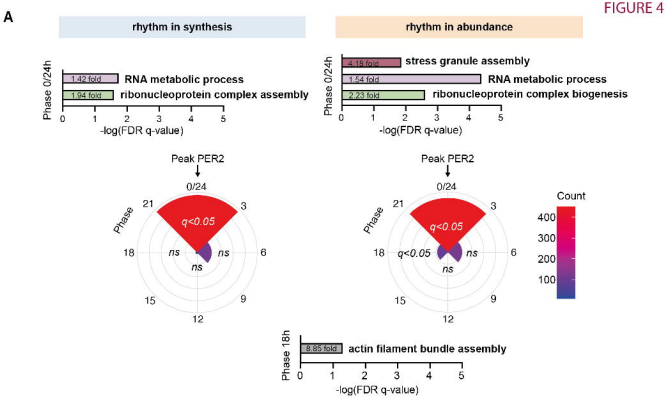
A
rhythm in synthesis
rhythm in abundance
Phase 0/24h
1.42 fold
RNA metabolic process
1.94 fold
ribonucleoprotein complex assembly
-log(FDR q-value)
4.18 fold
stress granule assembly
1.54 fold
RNA metabolic process
2.23 fold
ribonucleoprotein complex biogenesis
Peak PER2
0/24
Phase
q<0.05
ns
Count
Phase 18h
8.85 fold
actin filament bundle assembly

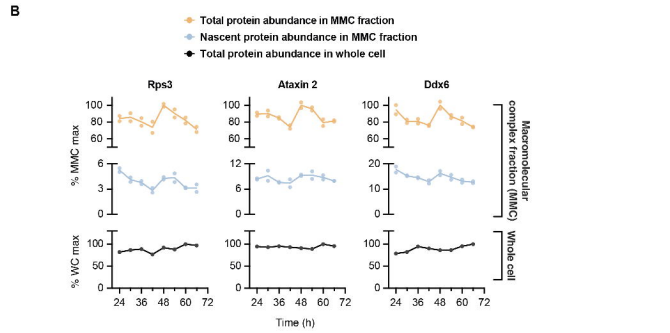
B
Total protein abundance in MMC fraction
Nascent protein abundance in MMC fraction
Total protein abundance in whole cell
Rps3
Ataxin 2
Ddx6
% MMC max
% WC max
Macromolecular complex fraction (MMC)
Whole cell
Time (h)

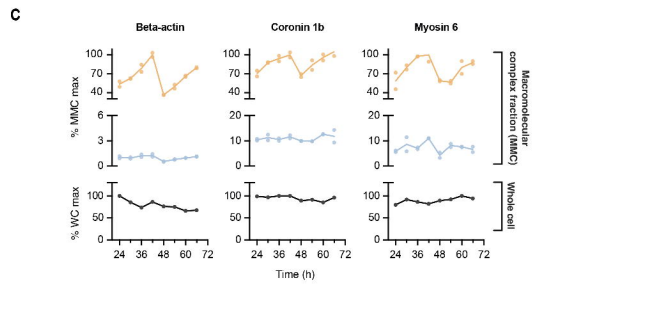
C
Beta-actin
Coronin 1b
Myosin 6
% MMC max
% WC max
Macromolecular complex fraction (MMC)
Whole cell
Time (h)

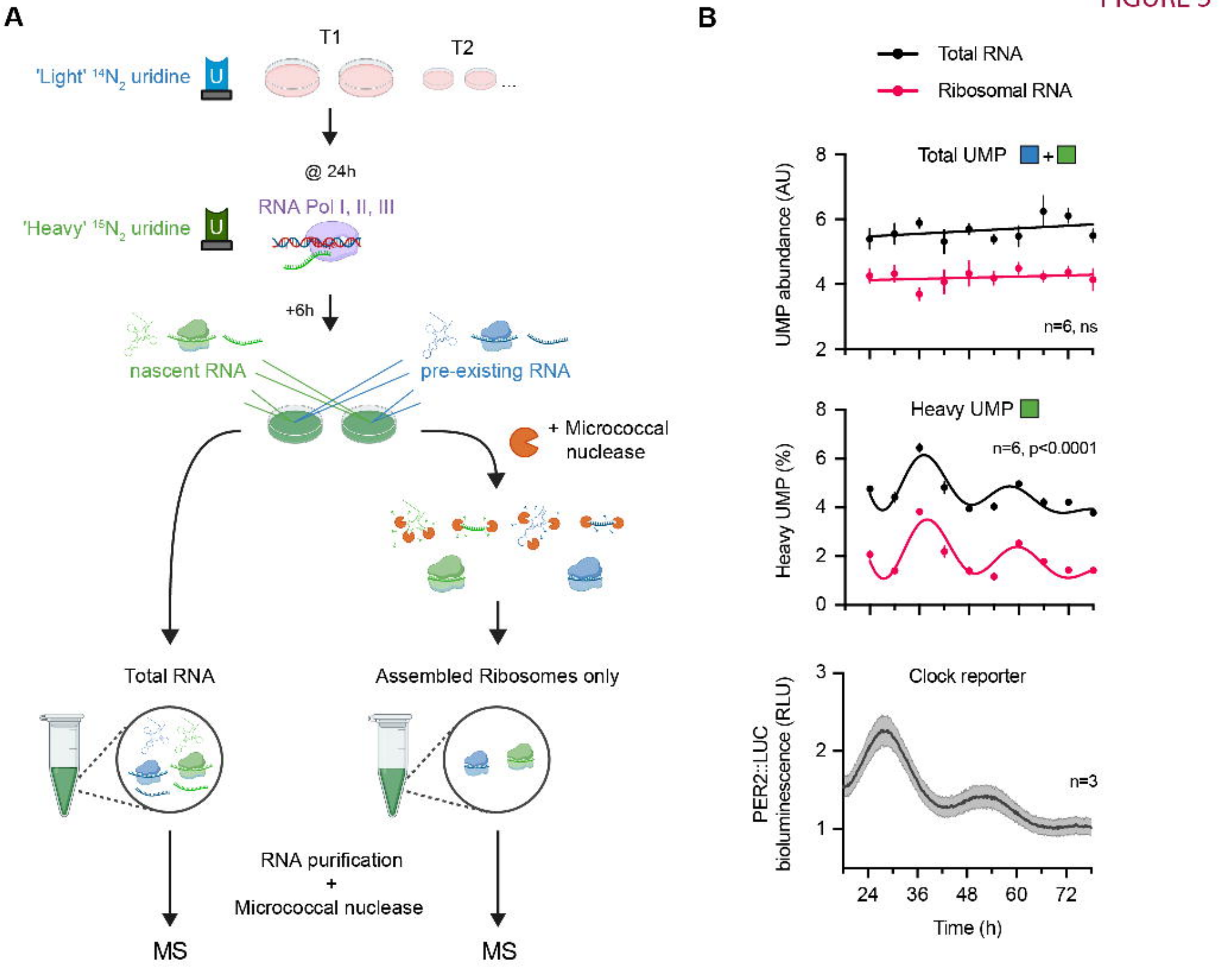
A
T1
T2
'Light' $^{14}N_2$ uridine
U
@ 24h
RNA Pol I, II, III
'Heavy' $^{15}N_2$ uridine
U
+6h
nascent RNA
pre-existing RNA
+ Micrococcal nuclease
Total RNA
Assembled Ribosomes only
RNA purification
+
Micrococcal nuclease
MS
MS
B
Total RNA
Ribosomal RNA
Total UMP
+
UMP abundance (AU)
n=6, ns
Heavy UMP
Heavy UMP (%)
n=6, p<0.0001
Clock reporter
PER2::LUC bioluminescence (RLU)
n=3
Time (h)

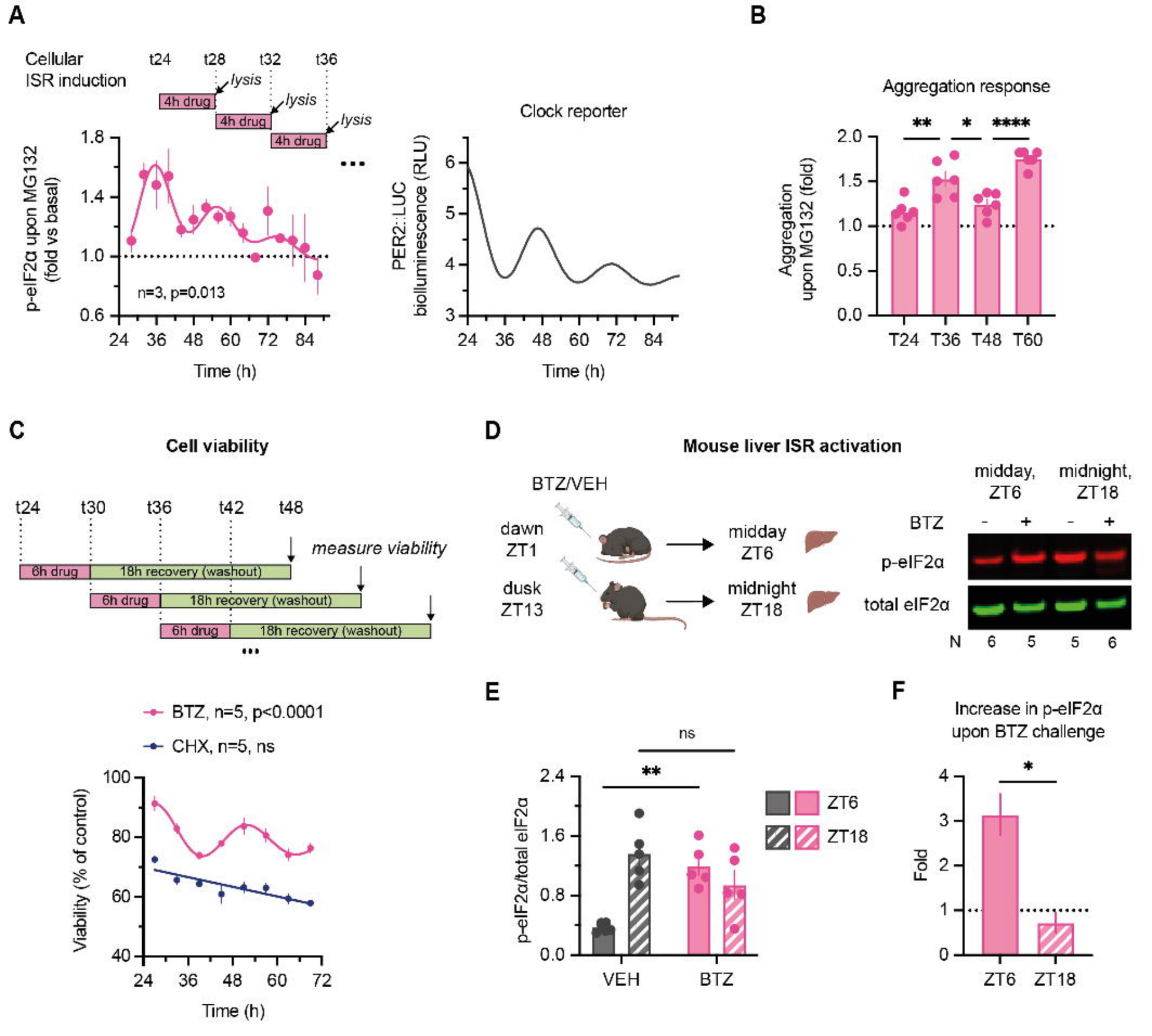
A
Cellular ISR induction
t24
t28
t32
t36
lysis
4h drug
p-eIF2α upon MG132 (fold vs basal)
n=3, p=0.013
Time (h)
Clock reporter
PER2::LUC bioluminescence (RLU)
Time (h)
B
Aggregation response
Aggregation upon MG132 (fold)
**
*
****
T24
T36
T48
T60
C
Cell viability
t24
t30
t36
t42
t48
measure viability
6h drug
18h recovery (washout)
BTZ, n=5, p<0.0001
CHX, n=5, ns
Viability (% of control)
Time (h)
D
Mouse liver ISR activation
BTZ/VEH
dawn ZT1
dusk ZT13
midday ZT6
midnight ZT18
midday, ZT6
midnight, ZT18
BTZ
p-eIF2α
total eIF2α
N 6 5 5 6
E
ns
**
p-eIF2α/total eIF2α
ZT6
ZT18
VEH
BTZ
F
Increase in p-eIF2α upon BTZ challenge
*
Fold
ZT6
ZT18